Lunds Universitets Naturgeografiska Institution

Seminarieuppsatser Nr. 72

The usefulness of coarse resolution satellite sensor data for identification of biomes in Kenya

Lova Cronquist & Sofia Elg

2000

Department of Physical Geography,
Lund University
Sölvegatan 13, S-221 00 Lund,
Sweden

Abstract

Vegetation phenology (seasonal rhythm) is closely related to seasonal dynamics in the lower atmosphere and is therefore an important element in global climatic models and vegetation monitoring. Remote sensing is the primary means by which we can observe the dynamic characters of the earth's biosphere. Description and mapping of the natural vegetation, and its interpretation in terms of soil, climatic and other information, are important in land use planning, particularly in areas where detailed information on soil and climate is insufficient, as is often the case in East Africa. The aim of this study is to investigate the usefulness of coarse resolution (1 km) data from the NOAA AVHRR sensor for the identification and separation of principal vegetation communities (biomes) and to define seasonal rhythms for these communities.

The Advanced Very High Resolution Radiometer (AVHRR) sensor is carried by a series of meteorological satellites operated by the National Oceanic and Atmospheric Administration (NOAA). The primary advantage of the AVHRR is the frequent temporal (daily) coverage over large areas, which allows a better opportunity to obtain cloud free coverage during important phenological stages. Normalised Difference Vegetation Index (NDVI) data derived from AVHRR offer a means of evaluating phenological characteristics, such as flowering and senescence. A total of 53 AVHRR NDVI composites covering Kenya between 1 April, 1992 and 21 September, 1993, were obtained from National Aeronautics and Space Administration (NASA).

The results show that some essential biomes such as grassland and dry forest were possible to identify and separate. Phenological characteristics, such as beginning and end of growing season were only possible to extract for grassland and dry forest. Even though cloud detection and interpolation methods were applied on the composites, the influence of clouds degraded the image quality and it was therefore difficult to interpret the NDVI profiles.

This study indicates the potential usefulness of 1-km NOAA data for monitoring vegetation phenological cycles and has demonstrated that atmospheric effects (e.g. clouds) must be understood quantitatively for specific inventory purposes.

The usefulness of coarse resolution satellite sensor data for identification of biomes in Kenya

Table of contents

1 INTRODUCTION

Natural vegetation rarely exists in East Africa today. The influences of humans have more or less modified the vegetation over most areas accessible to their activities, such as agriculture, grazing of domestic stock, use of fire and, use of pesticides *e.g.* for bush clearing in tsetse infected areas (Lundgren 1975).

Knowledge about the ecological factors that determine the distribution of individual classification groups (taxa, Appendix II) and about the environment in which particular plant communities develop, will give the experienced farmer, forester or scientist indications about climatic and soil conditions. A plant community is an aggregation of plants with mutual interrelationships among each other and with the environment. Using this knowledge wisely, may prevent unnecessary mistakes in selecting suitable crops for an area, reduce costs for expensive soil investigations and compensate for the lack of detailed climatic information. Description and mapping of the natural vegetation, and its interpretation in terms of soils, climatic and other information, must therefore be essential parts of any land use planning operation, particularly in areas where detailed information on soil and climate is insufficient, as is often the case in East Africa.

Phenology is the study of the relationship between vegetative growth and environment. The phenology of a specific plant defines its seasonal pattern of growth, flowering, senescence and dormancy (Appendix II). Parameters that control phenology are temperature, hours of daylight and amount of precipitation. Remotely sensed images can expand the study from a specific plant to include overviews of vegetation communities or even entire biomes. A biome is defined as a climatically controlled group of plants and animals of a characteristic composition and distributed over a wide area, such as tropical rainforest, temperate grassland, desert, savannah and mountain habitats etc (Appendix II).

The Advanced Very High Resolution Radiometer (AVHRR, Appendix II) is a multispectral radiometer carried by a series of meteorological satellites operated by the National Oceanic and Atmospheric Administration (NOAA, Appendix II). They can acquire imagery over a swath width of approximately 2800 km, providing global coverage on a daily basis. Although AVHRR was designed primarily for meteorological studies, it has been successfully used to monitor vegetation patterns over broad geographical regions. The areal coverage of AVHRR is extensive enough to facilitate the direct observation and monitoring of entire biomes and major ecological zones.

AVHRR collects five channels of data at the spatial resolution of 1.1-km, the visible, near infrared and thermal infrared. A ratio can be formed between the visible and the near infrared data to create a “greenness“ index or vegetation index known as the Normalised Difference Vegetation Index (NDVI, Appendix II) (Chapter 4.5). High NDVI values reveals pixels dominated by high proportions of healthy vegetation. Non vegetated surfaces, including open water, human-made features, bare soil, and dead or stressed vegetation, will not have as high NDVI values as healthy green vegetation. Different biomes show different NDVI curves over time, NDVI profiles that can be used to separate biomes from each other. NDVI and other vegetation indices can provide a measure of the importance of vegetative reflectance over a surface.

Remotely sensed data always includes a certain amount of "noise", which represents variations that are not related to changes on the Earth's surface. Such variations may be the result of unpredictable variations in the performance of the system, such as that the satellite that carries the sensor is not always stable in its orbit around Earth. It may also be due to random elements from the landscape and atmosphere, such as the presence of clouds. Studies have been performed to detect clouds in AVHRR data (Kriebel 1996; Hutchison *et al*. 1995; Berger 1995; Stowe *et al*. 1991; Saunders *et al.* 1988). It is very important to estimate the amount of noise in remotely sensed data. If there is a large amount of noise, the image will not provide a reliable representation of the feature in interest.

Studies show that NDVI offer a means of efficiently and objectively evaluating phenological characteristics over large areas (Reed *et al*. 1994). Since NOAA satellites provide daily Earth observations, data from these have been used to extract NDVI profiles. Such profiles have been used to study the dynamics of major biomes (Malingreau, 1986; Malingreau & Tucker, 1988, 1989; Achard *et al.* 1990; Reed *et al.* 1994), to monitor vegetation (Tucker *et al*. 1984; Prince & Tucker 1986; Townshend & Justice 1990; Eklundh 1996), to monitor primary production (Tucker & Sellers 1986) and for land cover classification (Townshend *et al*. 1991).

In the study performed by Achard *et al.* (1990) the AVHRR 1.1-km resolution data have been used to assess the seasonal rhythms of the various vegetation types, which constitute the forest-savannah contact in West Africa. In the study, sampling sites are located in two zones, which have contrasting floristic, physiognomic, and seasonal features. The first zone includes two forest reserves where dense forest is the dominant vegetation type while the other zone mainly includes various tree and shrub savannahs. Achard *et al.* (1990) found that spectral responses are strongly influenced by prevailing atmospheric conditions. In this part of the world, the Harmattan wind during the dry season and the almost permanent cloud cover during the rainy season often degrade image quality. Separation of some vegetation types was possible, especially at certain periods of time. As expected, savannahs have a low NDVI during dry season. In wet areas it has not been possible to separate untouched semi deciduous forests from woody crops (often growing under degraded forests) from NDVI 1-km resolution (Achard *et al.* 1990).

Another study that was aimed to measure phenological variability from satellite imagery was the study performed by Reed *et al.* (1994). In this study, 12 vegetation measures (metrics) derived from 4 years of time-series NDVI data were developed to describe phenological phenomena of land cover types in the United States. These metrics include the onset of growing season, time of peak NDVI, maximum NDVI, rate of greenup, rate of senescence, and integrated NDVI. Measures of central tendency and variability of the metrics were computed and analysed for various land cover types. The goal was to assess the validity of the metrics and their potential for monitoring global environmental change. Results from the analysis showed strong coincidence between the satellite derived metrics and predicted phenological characteristics. In particular, interannual variability of spring wheat in North Dakota was identified, the phenology of four types of grasslands was characterised, the phenological fluctuations of shrublands was showed and the phenological consistency of deciduous and coniferous forests was established (Reed *et al.* 1994).

In a study by Reed and Schwartz (1999), phenological data derived from NOAA AVHRR was compared with modelled phenology. The study reports on initial efforts to link satellite and surface measurements of the green wave (also referred to as Start of spring Season, SOS) *i. e* the onset of spring, across a variety of land cover types in eastern United States.

Climatological data was used as input in Spring Index models to generate first leaf and first bloom surface phenology predictions for each station – year, 1991-1995. These data consisted of maximum and minimum temperatures from the Historical Climatology Network (HCN) Daily Temperature and Precipitation Data. The satellite data consisted of NDVI data from NOAA AVHRR. SOS dates were calculated for 10*10 km (100 pixels) windows centred on each HCN climate sites. Median SOS values for each land cover class and 100-pixel set were then associated with corresponding first leaf and first bloom Spring Index dates generated for each of the same station-years. The study showed that the satellite data–surface correlations were strongest for woodland classes, intermediate for tall grass, and weakest for short grass.

Early phenological studies during the 1980s and 1990s (Schwartz 1999 and references therein) introduced the process of maximum value composite (MVC, Appendix II) – a common way to compensate for cloud contamination by grouping the NDVI data in larger periods (typically 10 or 14 days), and retaining only the highest NDVI value from the arrays at each spatial location. But even with the maximum compositing process, not all clouds are removed and the presence of cloudy and mixed cloud-land pixels contaminates the data set.

2 AIM

The aim of this study is to investigate the usefulness of coarse resolution data from the NOAA AVHRR sensor for the identification and separation of biomes in Kenya, taking into consideration the influence of clouds on the quality of the remote sensing data.
The specific objectives of the study are to:

- Collect field information regarding the dominating species in homogeneous sites, which are large enough to be monitored by the NOAA AVHRR sensor.
- Extract temporal NDVI profiles from the NOAA AVHRR sensor that are representative for selected biomes
- Calibrate the phenological information with structural and functional characteristics of the biomes.

3 STUDY AREA

3.1 The country of Kenya

Kenya covers an area of 583,000 km^2, which includes around 13,600 km^2 of inland water, which represents a part of Lake Victoria. Kenya is positioned approximately between latitudes 5°0'N and 4°40'S and between longitudes 33°38'E and 41°75'E. It is bordered to the north by the arid bushlands and deserts of Ethiopia and Sudan, to the east by Somalia and the Indian Ocean, to the west by Uganda and Lake Victoria, and to the south by Tanzania (Figure 1). The main rivers in Kenya are the Athi/Galana and the Tana.

Figure 1. *Geographical setting of Kenya*

Two-thirds of Kenya's total area is classified either as a desert or semi-desert and only one-third is considered to be an arable land (Ojany & Ogendo 1988). Most of this arable land is found in the Kenyan Highland in central Kenya at elevation levels between 1,500 and 3,000 meters above sea level (m a.s.l.). The Great Rift Valley divides the Highlands into two parts (the Eastern and Western Highlands). This rift has an important influence on the different types of climate and ecological zones found within the county. The Highlands are classified as high-potential land, *i.e.* high-yielding and well suited for cultivation (Ojany & Ogendo 1988).

3.1.1 Elevation

The elevations vary from sea level to heights up to 5 200 meters above sea level at the highest peaks in the central highlands. This variation in altitude gives rise to a diverse physical environment, with characteristics varying from equatorial to alpine conditions (Ojany & Ogendo 1988). Elevation and topography determine local climatic conditions and moisture availability, and hence influence vegetation types and land-use conditions.

3.1.2 Climate and vegetation

The two seasonal monsoons, which bring the greater part of Kenya's rainfall, blow from the south-east during the first half of the year, and from the north-east during the second half (the direction changes as the sun moves across the equator). Large-scale topography, lakes and maritime effects produce a great diversity of regional and local climates. The seasonal displacements of several wind convergence zones, the trade winds, and the Atlantic and Indian Oceans all influence the region's climate. These geographical and meteorological factors create a pattern of rainfall, which changes markedly, both in amount and seasonally, over relatively small distances. Semi-arid climates prevail throughout most of the region, but the seasonal timing of the rains is highly localised. One reason for these large rainfall variations is the tremendous topological contrasts. The distribution and presence of large water bodies such as Lake Victoria and the Indian Ocean also affect the rainfall pattern (Ojany & Ogendo 1988).

Kenya consists of an enormous area of plains, which supports semi-desert vegetation. Although there are a number of outliers of the highland region scattered in various parts of it, the semi-desert region stretches to the north-east and east. Moist vegetation types cover the south-western quarter of Kenya. This part of Kenya consists mainly of the highland mass, including the Lake Victoria Basin to the west. A relatively moist tropical zone covers the coastal belt.

3.1.3 Soils

The central and western regions of the country consist of soils, which are derived from volcanic rocks. Most of these soils are well drained and deep. They include the nitisols, acrisols, luvisols, ferralsols, andosols and phaeozems. In the north, north-eastern and eastern part of the country are the shallow to deep, well-drained to poorly drained soils. These include the solonetz, solochaks, regosols, luvisols and cambisols. In the south and south-east are the soils developed on Basement System rocks. These mainly include the ferralsols, luvisols, acrisols and cambisols. The coastal area is characterised by the arenosols, fluvisols and luvisols (Lundgren 1992).

3.2 Sampling sites

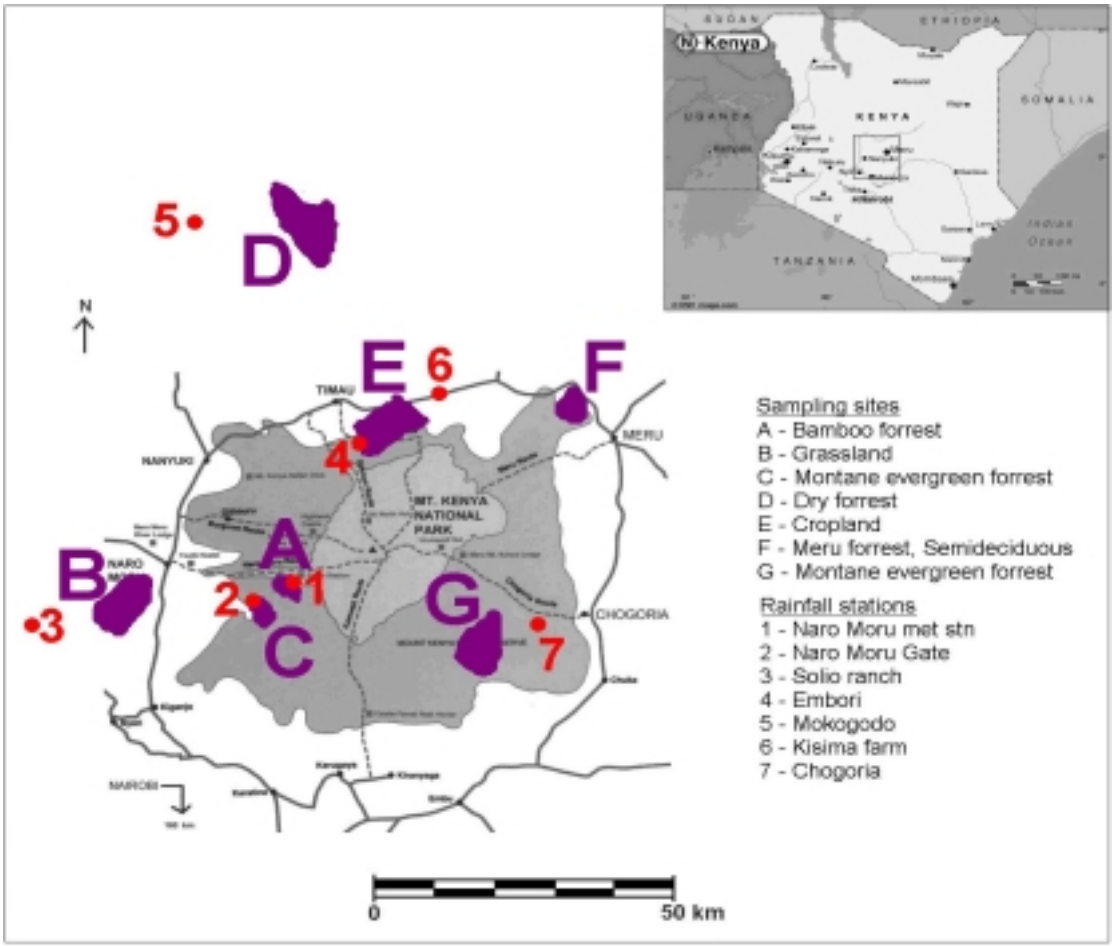

Figure 2. *The location of sampling sites and rainfall stations. The shaded area is Mount Kenya forest reserve.*

3.2.1 Sampling site A (bamboo)

- Location: the west slope of Mt Kenya
- Altitude: 3000 m a.s.l.
- Climate: Humid
- Rainfall: >1250 annual mm/year
- Temperature: max 18-22 C° min 10-14 C°

Figure 3*. Bamboo forest (Reader 1989)*

The mountain bamboo *Arundinaria alpina,* a member of the grass family, occurs in the altitudinal range 1800-3330 m. It appears to grow most vigorously where rainfall is plentiful and where the soils are relatively deep and the slopes not very steep. The tallest stems of *Arundinaria* grow to a height of 10-12 m or more and have slender branches covered with pale green leaves.

The plants do not grow in clumps but in dense even stands, Figure 3. The stems are often so close together such that it is difficult to pass through. The slender branches of the tops of the bamboo stems form fairly dense canopy so that vigorously growing bamboo has little in the way of under shrubs. Herbs, grasses, mosses and ferns form a large part of the ground cover.

3.2.2 Sampling site B (grassland)

- Location: Laikipia Plateau, west of Mt Kenya
- Altitude:1930 m a.s.l.
- Climate: Semi-arid
- Rainfall: 750-1200 annual mm/year
- Temperature: max 22-26 C° min 10-14 C°

Figure 4. *Grassland with Acacia*

The Acacia-grassland area is situated between two montane ranges; Mt Kenya and Aberdare range. This area is not pure grassland, almost 10% of the coverage is *Acacia molle,* figure 4. The dominant species is the perennial grass Red oat grass, *Themeda triandra*. Another grass that occurs is Kikuyo grass, *Pennisetum clandestinum.* Red oat grass is a tuft, perennial grass and 45-180 cm in height. The grass grows on latosolic soils of poor structure (Joseph K Mitugo, Laikipia Research Programme, personal communication). Minor rainfall peaks occur in April-May, July-August and November.

3.2.3 Sampling site C and G (montane evergreen)

- Location: the west and east slope of Mt Kenya
- Altitude: 1900 m a.s.l.
- Climate: sub-humid
- Rainfall: 1000-1600 annual mm/year
- Temperature: min 14-18 C° max 26-30 C°

Figure 5*. Montane evergreen forest with Black-barked camphor trees, rising 45m in height (Reader, 1989).*

The montane evergreen forest consists of three vegetation layers and is relatively dense, Figure 5. The west slope receives less rainfall than the east slope due to rain shadow. Main species found in the tree layer are camphor (*Ocotea)* trees and *Podocarpus*. The camphor tree is a massive, rough black-barked tree that can reach up to 45 m in height. *Podocarpus* is a slim coniferous tree.

3.2.4 Sampling site D (dry forest)

- Location: Mukogodo forest, Laikipia Plateau, north of Mt Kenya
- Altitude: 1900 m a.s.l.
- Climate: semi-arid, warm temperate
- Rainfall: 500-600 annual mm/year, bimodal
- Temperature: min 14-18 C° max 26-30 C°

The forest consists of two vegetation layers, one tree layer and one bush like layer. The trees have a height of 5-10 meter and the dominating species are *Euphorbia candelabrum, Olea africana,* and *Juniperus,* Figure 6. The rain falls in December-February and September-November.

Figure 6. *Mokogodo forest*

The Laikipia plateau is a zone of transition from the wetter to the drier part of the Eastern Kenyan Highlands. The area surrounding the Mokogodo forest is mainly covered with sparse grass and drought resistant *Euphorbia*. *Euphorbia* are found in very dry areas. Even during the very wet year 1998, when our field study was carried out, most riverbeds had dried up. Soil degradation and serious erosion are the main problems for the Mukogodo area, Figure 7.

Figure 7. *The area surrounding Mokogodo area, with an Euphorbia*

3.2.5 Sampling site E (crop land)

- Location: Laikipia Plateau, north of Mt Kenya
- Altitude: 2700 m a.s.l.
- Climate: semi-arid
- Rainfall: annual 720 mm/year
- Temperature: Temperature: min 14-18 C° max 26-30 C°

This area is dominated by large scale farming activities. Wheat and barley are shifted from year to year. In this area, artificial irrigation is necessary for these farming activities.

3.2.6 Sampling site F (Meru forest)

- Location: east slope of Mt Kenya
- Altitude: 1700 m a.s.l. (Meru town)
- Climate: Sub-humid
- Rainfall: annual 1360 mm/year (Meru town) + mountain mist
- Temperature: min 14-18 C° max 26-30 C°

The forest is evergreen and has very dense foliage with three to five layers of vegetation. Estimated coverage is 30% of trees, 25% of shrubs, 25% of herbs and 20% of climbers. The forest is a moist semideciduous, Figure 8. Vegetation is dominated by *Eleaodendron buchananii, Celtis africana* and *Celtis gomphophylla,* (Lind & Morrison 1974). Meru town is surrounded by dark red, clay, which is sensitive to erosion. This clay is highly fertile (Ojany & Ogendo 1988). The two major rainfall peaks are in April-May and November.

Figure 8. *Meru forest is semideciduous (Reader 1989).*

4 THEORETICAL BACKGROUND

4.1 The electromagnetic spectrum

All objects that have a temperature above the absolute zero emit electromagnetic radiation. Some objects also reflect radiation that has been emitted by other objects. By recording emitted or reflected radiation and applying a knowledge of its behaviour as it passes through the Earth's atmosphere and interacts with objects, it can be used to develop a knowledge of the characters of features (vegetation, structures, soils, rock, water bodies, etc.)

The most familiar form of electromagnetic radiation is visible light, which represents a small part of the full electromagnetic spectrum (Figure 9). The larger part of the spectrum lies outside the range of the human eye to apprehend.

Electromagnetic radiation approaches the Earth and passes through the atmosphere before it reaches the Earth's surface. Some of the radiation is reflected upward from the Earth's surface, and it is this radiation that makes out the basis for photographs and similar pictures. In addition, some solar radiation is absorbed at the Earth's surface and is redirected as thermal energy. Remote sensing systems that use reflected or emitted (thermal) energy are called passive systems. Active systems, like radar and laser that provide their own energy source, are also used in remote sensing.

As shown by Lillesand & Kiefer (1994), it is most common in remote sensing to categorise the electromagnetic waves by their wavelength location within the electromagnetic spectrum (Figure 9). Despite the assigned names such as ultraviolet or infrared, there is no clear-cut dividing line between these spectral regions; in contrast, the spectrum represents a continuum. The wavelengths of greatest importance for remote sensing purposes according to Swain & Davis (1978) are shown in the Table 1.

Table 1. *Important wavelengths in remote sensing.*

Spectral region	Wavelengths
Visible (VIS)	0.38 – 0.72 μm
Near infrared (NIR)	0.72 – 1.30 μm
Middle infrared (MIR)	1.30 – 3.00 μm
Far infrared	7.00 – 15.00 μm

Water vapour has a strong absorption at 6 μm. This is partly the reason why wavelengths between 3 and 7 μm is not commonly used. It is important to note that the infrared portion of the spectrum includes two completely different types of radiation: the near and parts of the middle infrared originate from the radiation of the sun, whereas the far infrared is directly related to the sensation of heat (thermal energy).

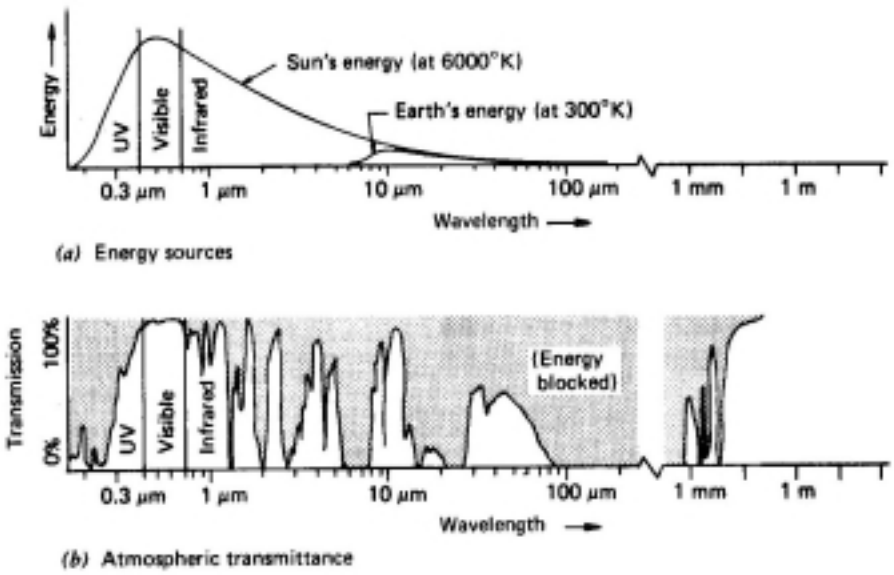

Figure 9. *Spectral characteristics of (a) energy sources, (b) atmospheric effects. The shaded area shows absorbed energy, the clear fields show in which wavelengths energy is transmitted through the atmosphere (Lillesand & Kiefer 1994).*

4.2 Atmospheric influence on radiation

Energy that reaches the satellite sensors must pass through the entire depth of the Earth's atmosphere. The atmosphere may have a profound effect on the quality of images and data that these sensors generate. These effects are mainly results from the mechanisms of atmospheric scattering and absorption (Figure 10). Scattering and absorption depends on the wavelength.

Scattering is the redirection of electromagnetic energy by particles suspended in the atmosphere or by large molecules of atmospheric gases. It can be divided into three different categories, according to the relationship between the wavelength of the radiation and the size of the particles causing the scattering;

- Rayleigh scattering is caused by atmospheric molecules and other tiny particles that are much smaller in diameter than the wavelength of the interacting radiation. There is a much stronger tendency for short wavelengths to be scattered by this scattering mechanism than long wavelengths.

- Mie-scattering exists when the diameters of atmospheric particles essentially equal the energy wavelengths being sensed. Water vapour and dust are major causes of Mie scatter and can influence a broad range of wavelengths in and near the visible spectrum. The strength of this effect depends strongly on the scattering direction and the viewing angle, satellite-zenith angle and relative azimuth between sun and satellite.

- Nonselective scattering is caused by particles that are much larger than the wavelength of the scattered radiation. For radiation in and near the visible spectrum, such particles might be larger water droplets, or large particles of airborne dust. This type of scattering is not wavelength dependent.

In contrast to scattering, atmospheric absorption results in effective energy loss to the atmospheric components. Energy is absorbed at given wavelengths, at the so-called band of absorption. The most efficient absorbers of solar radiation are water vapour, carbon dioxide, and ozone (Lillesand & Kiefer 1994). For water vapour, there is a strong absorption at 1.4, 2 and around 3 and 6 μm. Carbon dioxide strongly absorbs radiation at 15 μm, and weaker at 2.5 μm and 4.5 μm. Energy of 0.1-0.3 μm and 0.32-0.36 μm wavelengths is absorbed by ozone (O_3).

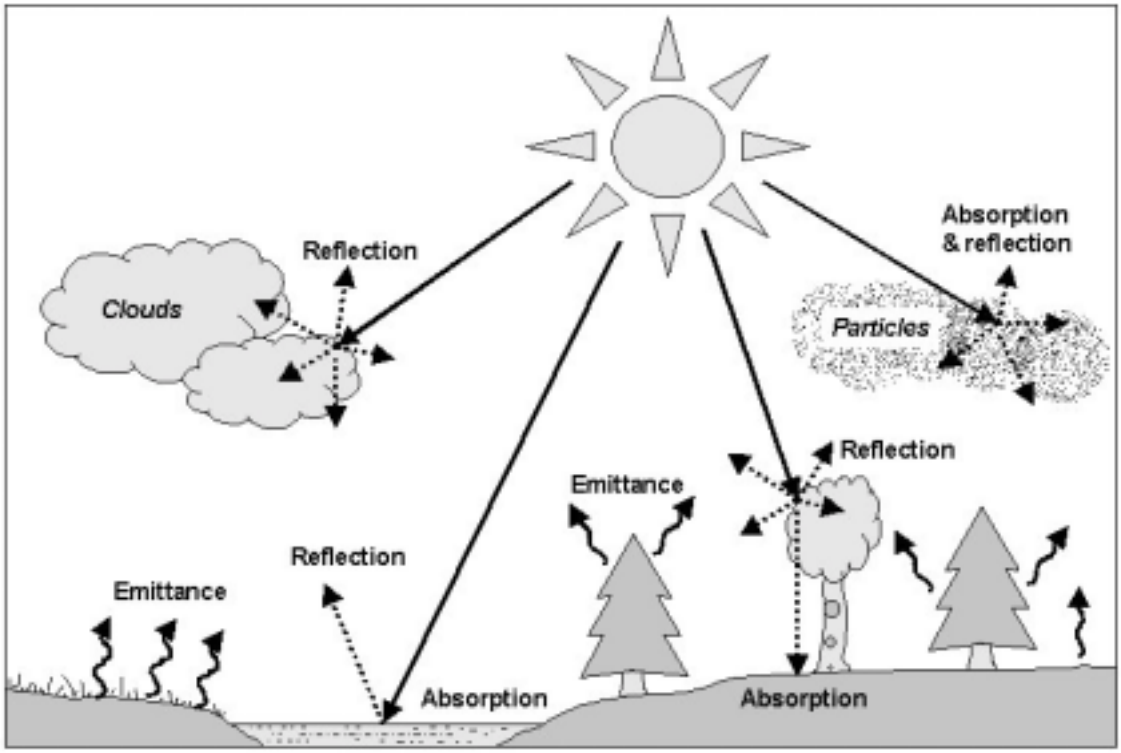

Figure 10. *Incoming energy can be reflected and absorbed. Energy is reflected by cloud, atmospheric particles and by ground cover. Energy is absorbed by atmospheric gases and ground cover. Some of the absorbed energy is emitted back to the atmosphere as thermal energy (modified from, Nämden för skoglig fjärranalys).*

The atmosphere selectively transmits energy of certain wavelengths; those wavelengths that are relatively easily transmitted through the atmosphere are referred to as atmospheric windows (Figure 11). The atmospheric windows are of high significance for remote sensing as they define those wavelengths that can be used for forming images.

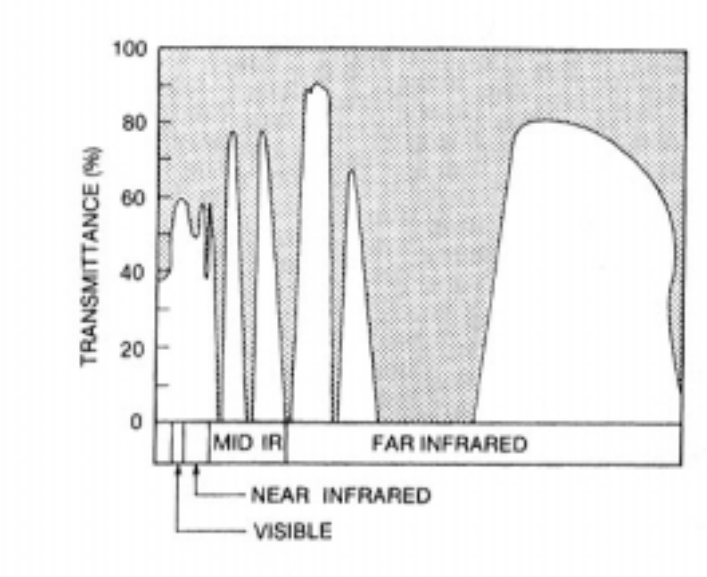

Figure 11. *This figure shows a schematic representation of atmospheric windows, the clear areas. The shaded area represents absorption of electromagnetic radiation (Campbell 1996).*

4.3 Spectral reflectance of the surface

When electromagnetic energy strikes any given feature on the Earth surface, three types of interaction are possible: reflection, absorption and/or transmission. The reflected component is important for remote sensing purposes because this sort of radiation can be measured by the sensor system. The reflected energy is equivalent to the incident radiation on a given feature minus the energy absorbed and/or transmitted by that feature. The reflection of a certain surface depends on different factors. The most important ones include (Roth 1997):

- Nature of the material
- Physical condition (*e.g.* wet – dry, healthy – stressed)
- Surface roughness of the object
- Exposure to the sun and solar elevation angle
- Spectral features (colour tone) of the object

The amount of reflected energy varies not only with different materials but also with the same materials in having different conditions. Furthermore, as far as a single feature type is concerned, its reflection varies at different wavelengths. As a consequence, each surface material has its characteristic reflection over a range of wavelengths, which corresponds to the so-called spectral signatures or profiles (Figure 12).

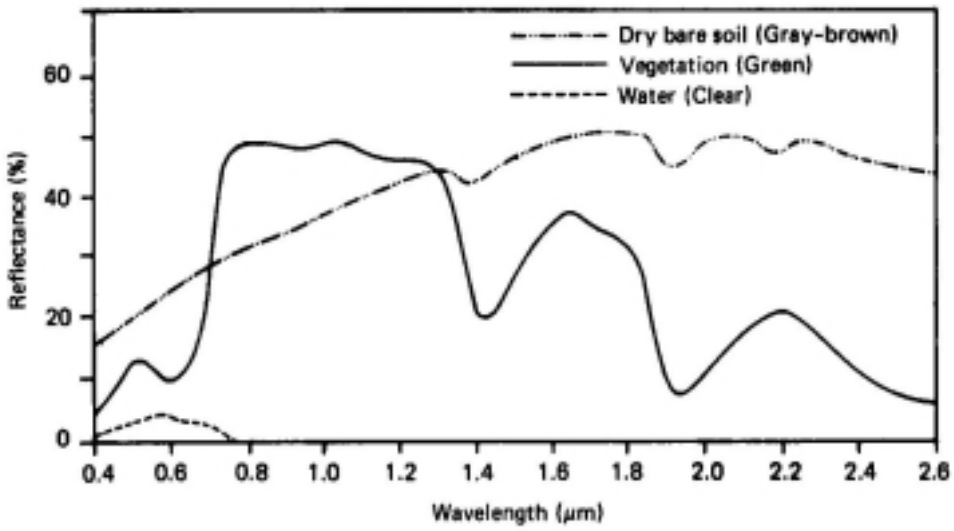

Figure 12. *Typical spectral reflectance curves for vegetation, soil and water (Lillesand & Kiefer 1994)*

Reflection characteristics of a surface are described by the bidirectional reflectance distribution function (BRDF, Appendix II). The BRDF is a mathematical description of the optical behaviour of a surface with respect to angles of illumination and observation (Campbell 1996). The bidirectional effect deals with the dependence of reflectance on sun-target-sensor geometry. For many geophysical applications, such an effect must be accounted for in the use of remote-sensing data based on BRDF's (Cihlar *et al.* 1996).

The recognition of distinct spectral profiles is the key to most procedures for computer-assisted interpretation of remote sensing data. However, the differentiation is not always given as clearly as in figure 12. The profiles of two feature types may intersect with one another in one spectral range but differ greatly in another wavelength band.

The spectral characteristics of a feature may be altered according to seasonal variations or geographic locations. Regarding the temporal effects, the same land cover type in a dry season may look very different during a rainy season. The spatial effects are also important because some features show different spectral characteristics at different geographic locations, which vary in terms of because soil types, climate, or cultivation practices.

In the following paragraphs, the spectral reflectance curves of vegetation and soil will be examined in order to describe their general characteristic features.

4.3.1 Vegetation

The reflection curve of green vegetation varies considerably with wavelength (Figure 13). The strong absorption by leaf pigments – particularly chlorophyll – in the blue (0.4 μm) and the red (0,6 μm) regions of the visible spectrum leads to the characteristic of green appearance in healthy vegetation. The light absorbed in the red and blue bands provides energy for the process of photosynthesis. In the near infrared (NIR) region (between 0.7 and 1.3 μm), the reflectance rises sharply because green leaves absorb very little energy, due to the internal leaf structure. It is often possible to distinguish between species in this range of the spectrum, according to the variations in their leaf structures. It is important to note that, in comparison to

the reflectance from a single leaf, multiple layers of leaves in a plant canopy can cause an even higher reflectance in the NIR, due to additive reflectance (Swain & Davis 1978). The maximum reflection is reached at about six to eight leaf layers. In the middle-infrared region, the water absorption bands at 1.4, 1.9 and 2.7 μm reduce the reflection because the water in the leaves absorbs strongly. The amount of absorbed energy increases with moister content and thickness of the leaves.

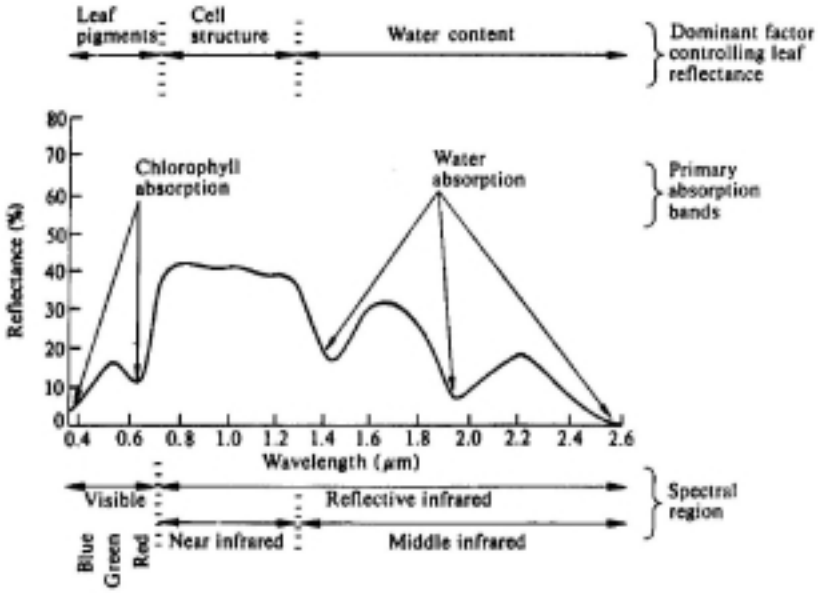

Figure 13. *Typical reflectance curve of green vegetation (Lillesand & Kiefer 1987)*

As soon as leaves loose moisture (*e.g.* in stress), the reflection from the vegetated area decreases. When leaves senescent there is a decrease in infrared reflection caused by deterioration of the cell wall. Also the chlorophyll starts to break down and as a result, the reflectance in blue and red wavelengths increases (Figure 14).

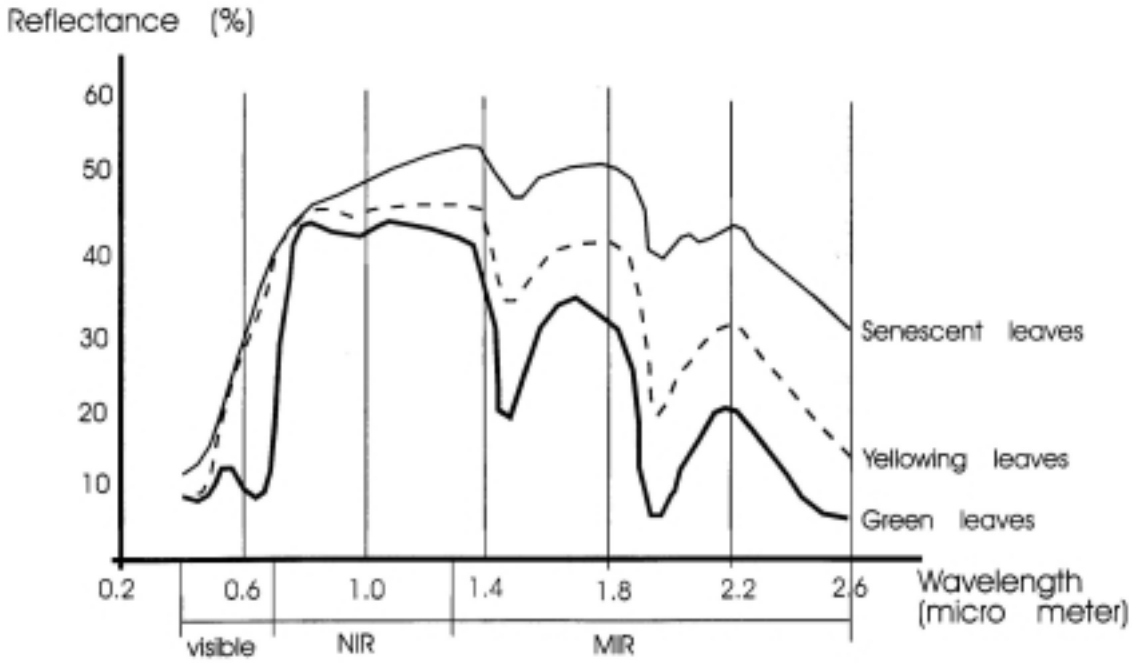

Figure 14. *Spectral reflectance of leaves in different conditions registered by NOAA (Swain & Davies 1978).*

4.3.1.1 Grasslands

Grasses can be considered mainly perennials that annually shed photosynthetic tissue and respond rapidly to environmental factors such as day length, water in the soil and temperature. Biomass reaches its maximum in summer, but the vegetation response can be unpredictable because it depends on rainfall events. In addition, variations in the precipitation regime, especially at drier sites, during any particular season are readily reflected in productivity (Reed *et al.* 1994).

4.3.1.2 Forests

Photosynthetic activity in deciduous forests depends on the amount of sunlight, moisture and temperature to which the forests are exposed. A typical spectral signature for deciduous forests starts from a minimum in the winter followed by a rapid increase to a maximum by late spring, lasting at a maximum level for about two or three months, then decreasing steadily until defoliation in autumn. Evergreen forests differ primarily from deciduous pattern in that a low rate of photosynthesis persists in winter. The patterns of photosynthesis activity are mainly a function of temperature and sunlight, which are relatively stable from year to year, and thus the interannual variations over both deciduous and evergreen forests are expected to be relatively low (Reed *et al.* 1994).

4.3.2 Soil

The soil reflection curves are generally less complex in appearance than those of vegetation (Figure 12). A characteristic feature of soil is the rise in reflectivity with increasing wavelength, particularly in the visible and near-infrared portion of the spectrum. Although the reflectance curves of most soils are very similar in their general shape, they can be affected by various factors, such as moisture content, soil texture (proportion of sand, silt and clay),

surface roughness, amount of organic matter, and presence of iron dioxide (Lillesand & Kiefer 1994). All these factors are complex, variable, and closely interrelated. For example, the presence of moisture in soil reduces its reflectance. Further, the soil reflectance is reduced by surface roughness, content of organic matter and iron dioxide.

When satellite sensors collect digital data, the reflection of vegetation is often mixed with that of soil surface. This may become a problem with vegetation types such as grassland, where the reflection from vegetation is closely mixed with bare soil (Campbell 1996). Dry, bright soil tends to have high reflectance in both the red (0.6 μm) and near infrared regions (0.72 – 1.30 μm), compared to living vegetation, which has a high reflectance in near infrared region but low reflectance in the red region (Figure 12). In the near infrared, the soil reflectance is lower than the green vegetation (Ringrose *et al*. 1989).

4.4 Satellite sensors used in the study

4.4.1 The Advanced Very High Resolution Radiometer

The Advanced Very High Resolution Radiometer (AVHRR) is a multispectral radiometer carried by a series of meteorological satellites. The sensor AVHRR is operated by National Oceanic and Atmospheric Administration (NOAA) of the USA in near polar and sun-synchronous orbits. A satellite in a sun-synchronous orbit carries the satellite track westwards at the rate that compensates for the change in local sun time as the satellite moves from north to south. Therefore, the satellite observes each scene at the same local sun time, removing time of day as a source of variation in light. Although AVHRR was designed primarily for meteorological studies, it has been successfully used to monitor vegetation patterns over broad geographic regions (Campbell 1996). Area cover is extensive enough that entire biomes, or major ecological zones, can be directly observed and monitored in a way that previously was not feasible. The primary advantage of the AVHRR is the frequent temporal (daily) coverage over large areas, which allows a greater opportunity for obtaining cloud-free coverage during important phenological stages of the land cover.

The satellite makes about 14 passes in a 24-hour period at a height of 833 km, collecting data for each 2800-km swath twice daily, at 12-hour intervals (Table 2). Because of the wide-angular field of view (+-55.4 degrees), areas recorded near the edges of the image suffer from severe geometric and angular effects. As a result, AVHRR data selected from the regions near the nadir provide the most accurate information (Campbell 1996). Nadir is the point on the surface that is exactly underneath the centre of the lens in the sensor (Appendix II). At nadir NOAA AVHRR has a spatial resolution of 1.1 km.

AVHRR collects five channels of data, one in the visible, one in the near infrared, and three in the thermal infrared wavelength (Table 3). It is mainly channels 1 and 2 that are used in vegetation studies (Figure 15).

Table 2. *Characteristics of AVHRR.*

AVHRR characteristics	Data
Scan angle	+/- 55.4 degrees
Pixel size (ground resolution)	1.1 km
Swath width	2400 km
Temporal resolution	12 hours

Table 3. *Spectral Channels for AVHRR.*

Channel	Spectral region	Wavelengths μm
Channel 1	Visible (green-red)	0.58 – 0.68
Channel 2	Near infrared (NIR)	0.72 – 1.10
Channel 3	Middle-far infrared	3.55 – 3.93
Channel 4	Far infrared	10.5 – 11.5
Channel 5	Far infrared	11.5 – 12.5

Channel 1 and 2 are used to identify clouds, land, water, snow and ice coverage. Channel 3 registers atmospheric water vapour and high temperatures. Surface temperature of a water body or clouds can be calculated from channels 4 and 5.

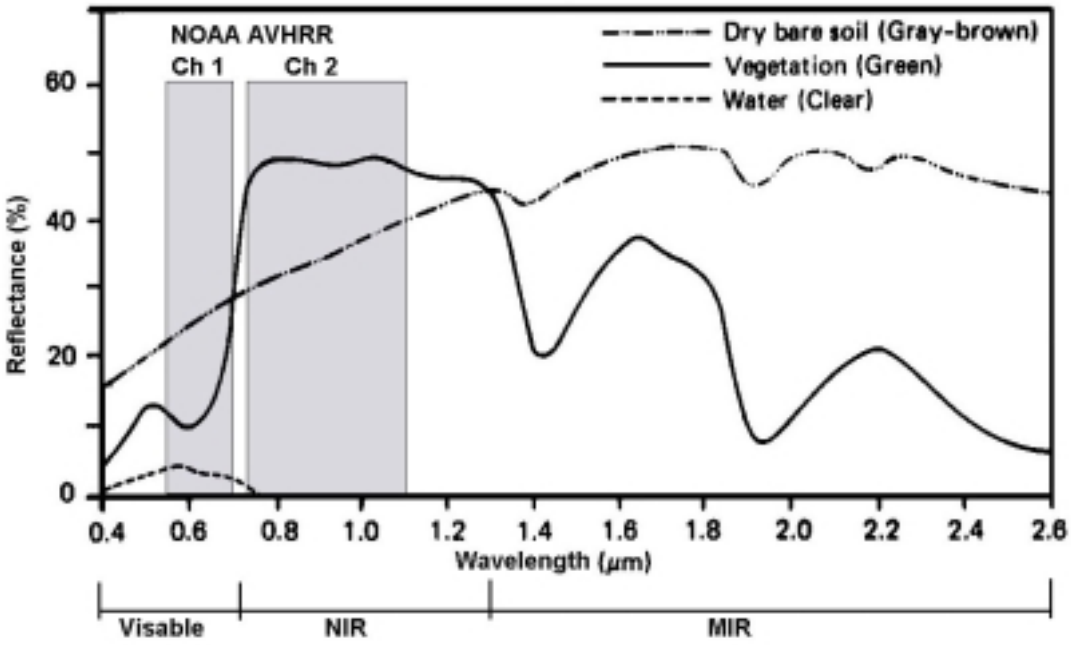

Figure 15. *The spectral signatures for soil, vegetation and water shown together with NOAA AVHRR channel 1 and 2 (modified Lillesand & Kiefer 1994).*

4.4.2 Landsat MSS sensor

The Multispectral Scanner, MSS (Appendix II), onboard the satellite Landsat covers a 185-km swath width. MSS register data in four wavelength bands; green and red in the visible spectrum and two in the near infrared. The satellite is in a near-polar sun-synchronous orbit with a ground-track speed of 6.47 km/s. The MSS scans each line from west to east with the southward motion of the spacecraft providing the along-track pole to pole progression of the

scan-lines. The characteristics and spectral channels for Landsat MSS are listed in table 4 and 5.

Table 4. *Characteristics of Landsat MSS*

Landsat MSS characteristics	Data
Scan angle	11.56 degrees
Pixel size (ground resolution)	79 m
Swath width	185 km
Temporal resolution	18 days

Table 5. *Spectral Channels for Landsat MSS*

Channel	Spectral region	Wavelengths μm
Channel 1	Green	0.5-0.6
Channel 2	Red	0.6-0.7
Channel 3	Near infrared (NIR)	0.7-0.8
Channel 4	Near infrared (NIR)	0.8-1.1

4.5 Normalised Difference Vegetation Index (NDVI)

Various mathematical combinations of the AVHRR channels 1 and 2 have been found to be sensitive indicators of the presence and conditions of green vegetation, referred to as vegetation indices. The simplest form of vegetation index is a ratio between two digital values from separate spectral bands. For living vegetation, the ratio strategy can be especially effective because of the inverse relationship between the spectral reflection of vegetation in the red and infrared region. The fact that photosynthetically active vegetation absorbs red light and reflects near infrared radiation, caused by internal cell structure (Figure 13), means that if we form a ratio between these two spectral bands, it will become very sensitive to variations in the amount of chlorophyll on the ground. One of these vegetation indices is the Normalised Difference Vegetation Index (NDVI) and is normally calculated as follows (Campbell 1996):

NDVI = (NIR – Red) / (NIR + Red)

where NIR is the spectral radiance in the near infrared channel (NOAA channel 2) and Red is the spectral radiance in the visible red channel (NOAA channel 1), Figure 15.

The NDVI equation theoretically produces values in the range of –1.0 to 1.0 (Tucker 1979), where the positive values indicate increasing green vegetation and negative values indicate non vegetated surface features such as water, barren, ice, snow or clouds. For computational and storage reasons, the NDVI values are usually transformed to values between 0 and 200 and truncated. By looking at spectral reflectance for vegetation using NDVI images, NDVI profiles can be extracted over time and used to separate different biomes.

4.6 Sources of error

One of the most important procedures in the use of AVHRR data for land applications is to ensure that derived parameters (*e.g.* NDVI and surface temperature) are representative of the land surface. All remote-sensing systems generate geometric errors, either systematic or

random, that have to be taken into consideration. These errors mean that the representations of positions and shapes of features do not match reality on the Earth's surface and corrections must be made before use of data. There may also be elements in the atmosphere, such as atmospheric gases and clouds, that affect the gathered data.

4.6.1 Sensor-related variations

Systematic variations in the remote-sensing system can be caused by the rotation of the Earth, scanning time and scanning angle. These variations can be calculated and corrected by mathematical models.

Errors due to the rotation of the Earth are; (1) differences in speed between the satellite and the rotation of Earth, and (2) differences in speed of Earth rotation around its own axis. The fact that the equator rotates faster than the speed at the poles causes displacement in east-westerly direction between the first and the last row of a satellite scene.

A sensor has a certain scanning time, meanwhile the satellite moves in its orbit direction, causing the first pixel to be slightly behind the last pixel in a raw data image.

Although the sensor rotates at a constant speed, the projection of the instantaneous field of view (IFOV, Appendix II), on the ground surface does not move (relative to the ground) at the same speed because of the varied distance from the satellite to the surface. At nadir the sensor is closer to the ground than it is at the edge of the image and therefore the sensor scans a shorter distance at nadir than it does at the edge of the image. This is why the scanner produces a geometric error that tends to compress features along an axis parallel to the scan lines.

There is an increase in relief displacement with increasing scanning angle. At the centre of the image the sensor views objects directly below and the position in the image is correct. However, as the distance from the middle increases, the sensor views the sides rather than the top of features on the ground and relief displacement increases.

The bidirectional effect plays an important role in remote sensing because it deals with the dependence of reflectance on sun-target-sensor geometry. In the case of AVHRR, the dependence is of special interest because of the wide scanning range of the sensor. The scan angle has a profound effect on the radiometry because of the fact that the surface does not reflect energy equally in all directions and because of the influences from the atmosphere (Eklundh 1996).

Random variation can be caused by satellite instability, and the errors cannot be corrected by mathematical models. Therefore, a comparison with surface ground truth must be made.

Instability in the satellite orbit such as variation in altitude and speed causes scale alterations respectively differences in scanning width. As the satellite rolls and pitches, the scan lines loose their correct positional relationships.

4.6.2 Atmospheric influences

The atmosphere affects the reflectance of surface features measured from the sensor through scattering and absorption of solar radiation by atmospheric gases. The NDVI dataset used in this study are corrected for ozone and Rayleigh scattering but not for water vapour and aerosols.

The effect of clouds on surface reflectances is of major importance. For example, a small or thin cloud within the instantaneous field of view (IFOV) of a land surface pixel may significantly reduce its calculated surface temperature or vegetation index. Cloud detection in satellite data relies essentially on the amount of spectral information given for each pixel. One broad channel in the visible region allows the satisfactory detection of bright cloud over the dark ocean but not over bright arid land surfaces. One channel in the 10 to 12 μm region (thermal) allows the satisfactory detection of high clouds because they are colder than the surface, but would not be able to distinguish low clouds from land surfaces (Kriebel 1996).

The AVHRR sensor was the first one to offer the possibility of two split-windows. This means that the visible/near infrared region is split into two channels, one below and one above 0.7 μm and the thermal infrared region is split into one channel around 11 μm and one around 12 μm. Additionally, a fifth channel at 3.7 μm is included in the AVHRR system.

Such enhanced spectral information offered by the AVHRR over previous sensors makes it possible to check each pixel separately according to its spectral properties, *i.e.* to apply a set of threshold tests to each pixel to determine the amount of cloud contained within it (see further section 6.4). The difficulty is in the setting of thresholds for particular regions and for particular seasons. Saunders and Kriebel (1988) have developed a sophisticated set of threshold tests in a package called APOLLO (AVHRR Processing scheme Over cLouds, Land and Ocean, Appendix II). The method utilises AVHRR channels 1 through 5 for separating clouds from other land features. The NOAA has also developed a sophisticated set of tests for clouds, called CLAVR (Clouds from AVHRR, Appendix II) (Stowe *et al.* 1991). Together, the APOLLO and CLAVR methods form the widely used set of cloud detection algorithms used world-wide. In this study we have used selected parts from APOLLO.

The basic idea of cloud detection is based on the apparent contrast between different channels in the measured radiances of cloud-free pixels. Clouds are bright in channel 1 and 2 *i.e.* they have high reflectance. In channel 4 and 5 they emit (heat) radiance according to their temperature (normally the temperatures of the viewed surfaces of cloud is very cold compared with sea or land surfaces). Clouds normally contrast strongly to the relatively darker and warmer land and sea surfaces, with the exception of low and thin clouds. Most cloud detection methods are based on the following characteristics of the Earth's surface (Kriebel 1996):

- The surfaces of oceans are dark in channel**s** 1 and 2 and warm in channel**s** 4 and 5
- Vegetated land is dark in channel 1, due to absorption of chlorophyll and little reflection, and bright in channel 2, due to high reflectance and also usually quite warm.
- Arid land is bright in channels 1 and 2.
- Normally snow and ice are very bright in channels 1 and 2 and relatively warm (in comparison to cloud temperatures) in channels 4 and 5.

From this generalisation, it follows that during the daytime, cold thick clouds can easily be distinguished from all kinds of other surfaces, except snow and ice, by setting a temperature threshold. However, warm thin clouds are difficult to be distinguished everywhere (Kriebel 1996).

5 MATERIAL

In this study we have used Landsat MSS with its high spectral resolution to select our study areas. The main dataset used in the phenological analysis was NOAA AVHRR 1.1 km dataset. Fifty three AVHRR NDVI images were used for studying phenology while AVHRR band 1, 2 and 5 were used for cloud detection. Additional data include: rainfall data, a vegetation map, reference data from fieldwork and information from local scientists.

5.1 NOAA AVHRR data

A total of 53 AVHRR NDVI composites covering Kenya between 1 April, 1992 and 21 September, 1993, were obtained from National Aeronautics and Space Administration (NASA). The major use of these composites was to study the surface vegetation cover over time.

The data were stored in Goodes Homolosine Interrupted Projection, which is an equal-area pseudocylindrical map projection. NASA has processed the 1-km dataset in steps that include radiometric calibration, geometric registration, compositing and atmospheric correction (Eidenshink *et al.* 1994, 1995). To avoid noise such as clouds, NASA processes 10-day composites. The raw data are processed into 10-day maxima. January has three composites of 10, 10, and 11 days; February has 10, 10, and 8 or 9 days depending on whether it is leap year, and so on. This procedure has the advantage of creating calendar month composites, which is a common reporting period for agronomic and biophysical characteristics (Eidenshink *et al.* 1994, 1995*).* For the NDVI composites, the method used by NASA is maximum value composite (MVC). In this method, the NDVI is examined pixel by pixel for each observation during the compositing period of 10 days to determine the maximum value, Figure 16 (Holben 1986).

Although the technique reduces cloud effects, the resulting composite data are usually not completely cloud-free. In areas of persistent cloudiness (*e.g.* tropical latitudes and some coastal areas), it is difficult to satisfactory remove cloud contamination through the maximum compositing method (Holben 1986). Previous work has shown that NDVI, and subsequently the MVC process, are a function of AVHRR scan angle (Holben & Fraser 1984; Moody & Strahler 1994), and using atmospherically corrected data in the MVC process may shift MVC selection toward high off-nadir positions (Zhu &Yang 1996 and references therein). Based on these findings the atmospheric correction was applied following the compositing process. The NDVI dataset used in this study are corrected for ozone and Rayleigh scattering but not for water vapour and aerosols (Eidenshink *et al.* 1994, 1995).

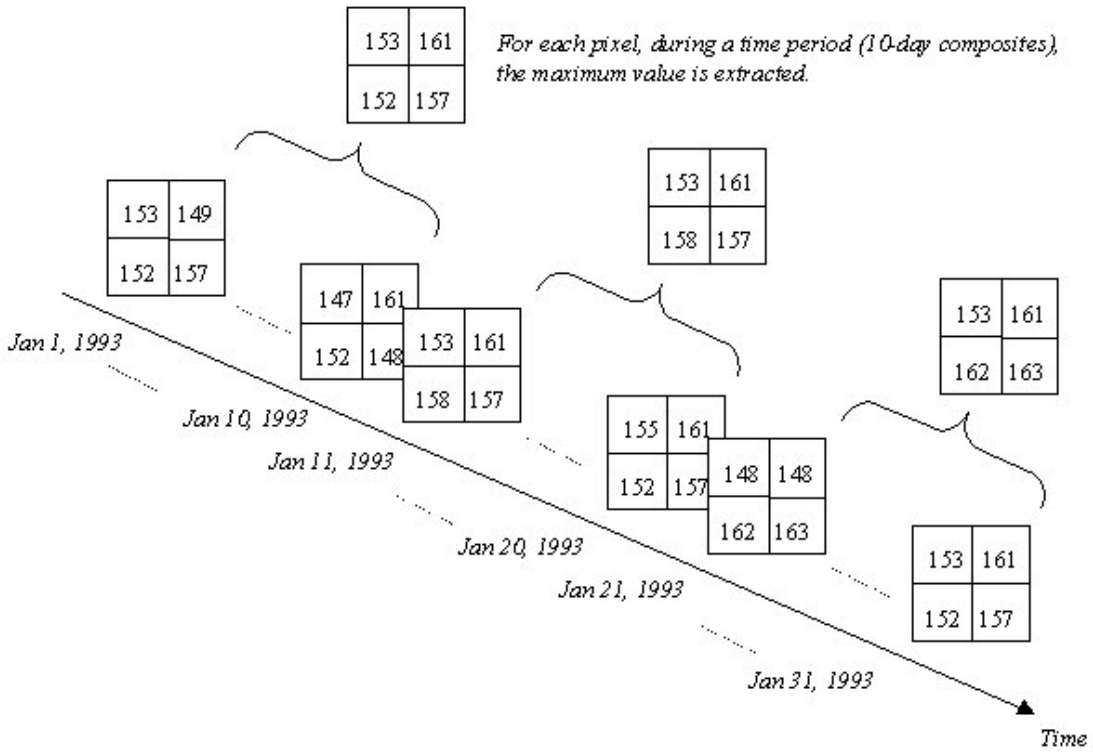

Figure 16. *The maximum NDVI value for each pixel over a 10-day period makes one 10-day composite*

5.2 Landsat MSS data

To locate appropriate sampling sites pre-processed (*i.e.* radiometrically and geometrically calibrated) Landsat MSS scene was used. The Landsat scene was taken on March 1989. Data were stored in Universal Transverse Mercator projection with ellipsoid WGS 84.

5.3 Rainfall data

Rainfall data were obtained from Laikipia Research Programme for the period 1991-1993 (Table 6). Some stations had no data for 1991. Daily precipitations were obtained from all stations and a 10-day and annual total for each station was calculated. The station locations are shown in Figure 2.

Table 6. *Rainfall stations. (NRM^3, Natural Resource Monitoring, Modelling and Management).*

No	Station name	X_coord (d:m:s)	Y_coord (d:m:s)	Elev. (m)
1	Naro Moru Met Stn	37°13’24’’E	0°10’07’’S	2990
2	Naro Moru Gate	37°08’48’’E	0°10’27’’S	2420
3	Solio ranch	36°52’43’’E	0°14’59’’S	1910
4	Embori (NRM^3)	37°18’53’’E	0°02’07’’N	2690
5	Mokogodo (NRM^3)	37°04’29’’E	0°23’23’’N	1750
6	Kisima farm	37°25’48’’E	0°07’12’’S	2410
7	Chogoria	37°35’23’’E	0°14’56´S	-

5.4 Software used

IDRISI software package (Eastman 1993) and programs developed for extracting signatures (Olsson & Eklundh 1994) were used for extracting NDVI data. For cloud detection, IDRISI was mainly used. The statistical software package SPSS was used for the interpolation of missing values after cloud pixels were eliminated. PCI Imageworks package (PCI 1994) was used to identify study areas from the MSS scenes.

6 METHODS

Cloud detection and interpolation methods were applied on 10-day NDVI composites to extract temporal profiles from each sampling site. A flowchart of the procedures and the methods used are shown in Appendix I. Field work was carried out for reference and ground truth.

6.1 Selection of sampling sites

The selection of sampling sites was critical for this study. The sampling sites were selected to include different biomes (vegetation compositions). It was important that the sites were larger than 1 km^2 and homogeneous, so that differences in spectral reflectance between the sampling sites could be explained by the functional differences of the vegetation. Kenya was chosen as study area because it still includes some larger natural vegetation communities, which have not yet been affected by humans. Seven sampling sites were chosen for this study, six of which contained different biomes, Figure 2.

6.2 Field work

For ground truth a fieldwork was carried out. At each sampling site one or more reference points were taken with a Global Positions System (GPS, Appendix II). At every reference point, a surrounding area of about 1 km^2 was viewed and the following data were documented if possible:

1. Co-ordinates (longitude, latitude, altitude)
2. Percentage degree of cover for the ground, bush and tree
3. Main species

In addition to these data, photographs were taken at each site and interviews with local scientists at the University of Nairobi were made, which later could support the identification of species.

6.3 Temporal NDVI profiles

Seven polygons, creating the boundary of each sampling site, were used to extract all pixel values represented in each polygon from the AVHRR NDVI data set. An average for each sampling site and for every 10-day composite was calculated creating a temporal NDVI profile (Appendix II) for the site. These profiles were extracted from both raw data (before cloud detection) and post-cloud detection data. For the calculation of the vegetation signature (Appendix II), the program Signature (Olsson & Eklundh 1994) was used. In the cloud detection procedure some pixels were deleted, because they were strongly influenced by clouds. The erased pixel values were replaced by interpolated values.

6.4 Cloud detection

Even though the maximum value composite (MVC) technique reduces cloud effects, the resulting composite data is usually not completely cloud-free (see previous section 5.1). In areas of persistent cloudiness (*e.g.* tropical latitudes and some coastal areas), it is difficult to

satisfactory remove cloud contamination through the maximum compositing method (Holben, 1986).

In cloud detection a classification to distinguish between cloud pixels and land surface was made and a cloud mask was calculated for each dataset. In a cloud mask land pixels were given the value one, while pixels contaminated with clouds were given zero. For assessment of cloud contamination in the NDVI composites of Kenya, a method adopted from APOLLO (Kriebel 1996; Saunders & Kriebel 1988) was used (previously explained in section 4.6.2.2). The method utilises AVHRR channels 1 through 5 for separating clouds from other land features. APOLLO consists of a total of five tests before a pixel is determined to be cloud free. In this study we have used selected parts from APOLLO. Two cloud tests were applied to each of the 53 10-day composites, the gross temperature test and the dynamic VIS/NIR ratio test. The gross temperature test uses AVHRR channel 5 based on the fact that most clouds have a lower temperature than the land surface. The dynamic VIS/NIR ratio test is based on the fact that most land surfaces have a much lower reflectance than clouds in channel 1. A flowchart, Appendix I, shows step by step the cloud detection approach.

6.4.1 Test 1 (Gross temperature test)

The first test applied is an infrared threshold test which uses the brightness temperature (surface temperature) calculated from NOAA AVHRR channel 5 (12 μm). Convective clouds, which are the most common clouds in tropical regions, can usually be detected using a temperature threshold. In contrast to the Earth's surface temperatures, convective clouds have much lower surface temperatures. A temperature threshold of +7°C (280 K) is set as threshold value. All pixels with temperatures less than 7°C are thus interpreted as cloud-contaminated.

In Figure 17a, the histogram shows infrared brightness temperature (thermal channel). The cloud-free land and sea peaks are well defined and the cloud-contaminated radiance is presented by a "cold" tail in the histogram.

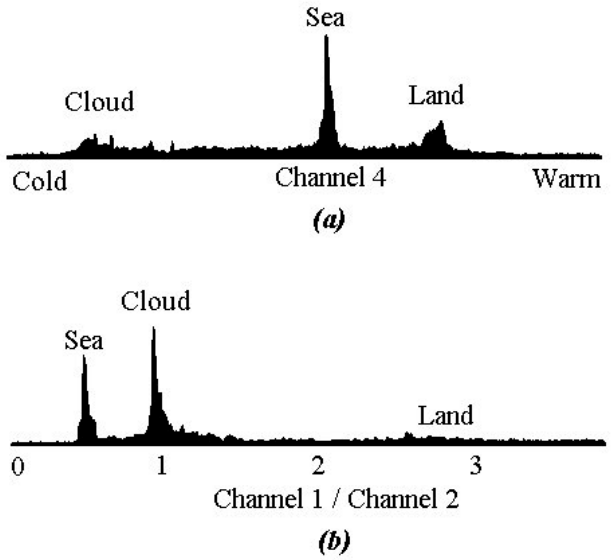

Figure 17. *Histogram of NOAA-9 AVHRR data shows an example of typical radiance values over land, sea and cloud (a) channel 4 brightness temperature, (b) channel 2/channel 1 reflectance ratio histogram (Saunders & Kriebel 1988)*

6.4.2 Test 2 (Dynamic VIS/NIR ratio test)

This test makes use of the reflectance ratio of channel 2, in the near infrared (NIR) region, and channel 1, in the visible (VIS) region. This ratio (Ch2/Ch1) should be close to 1.0 for clouds, as the reflectance of clouds only decreases slightly at near infrared wavelengths. Over land with healthy green vegetation, the reflectance increases markedly at the near-infrared wavelengths compared with the shorter ones. Even over desert or during the winter when the vegetation is dormant, the reflectance is higher at longer wavelengths (except over snow and ice), ensuring that the ratio value is always greater than 1.0 for the land surfaces. A pixel is classified as cloud free if the ratio is greater than 1.1 (Kriebel 1996).

Figure 17b shows the ratio between near infrared (Channel 2) and visible reflection (Channel 1). Now the cloud-free land radiance are well separated with a well-defined cloudy peak close to unity.

The result of each test is that every pixel is classified as either one (land) or zero (cloud). The result from tests 1 and 2 are then multiplied together on pixel by pixel basis. The product of that process represents our complete cloud mask. This mask is then multiplied with the original NDVI of every image resulting in new images where cloud contaminated pixels have the value zero while original NDVI remains the same in those pixels multiplied with one (classified as land) (Appendix I).

The estimation method used for replacing erased pixel values was linear interpolation (SPSS). The last valid 10-day composite value before the missing value and the first valid value after the missing value are used for the interpolation. If the first or last case in the series has a missing value, the missing value is not replaced.

To further reduce noise, a moving average over three 10-composites was calculated. For example an average for March 11, March 21 and March 31 was calculated and then an average for March 21, March 31 and April 1 resulting in a monthly moving average.

7 RESULTS

Figures 18-24 illustrate the results from the sampling sites A-G. NDVI is presented both as 'original NDVI' and as 'processed NDVI'. The X-axis presents time and the right Y-axis presents scaled NDVI. Original NDVI represents NOAA NDVI images before cloud detection and interpolation methods were carried out. Processed NDVI presents a moving average over three 10-day composites after cloud detection and interpolation methods were applied on the original datasets. By presenting monthly moving averages, the effect of noise was further reduced, but at the risk of losing information. Daily rainfall data were aggregated over 10-day periods for a better visual comparison between NDVI and rainfall. The left Y-axis represents rainfall data, Figures 18-24. The locations of precipitation stations in relation to the sampling sites are shown in Figure 2, page 11.

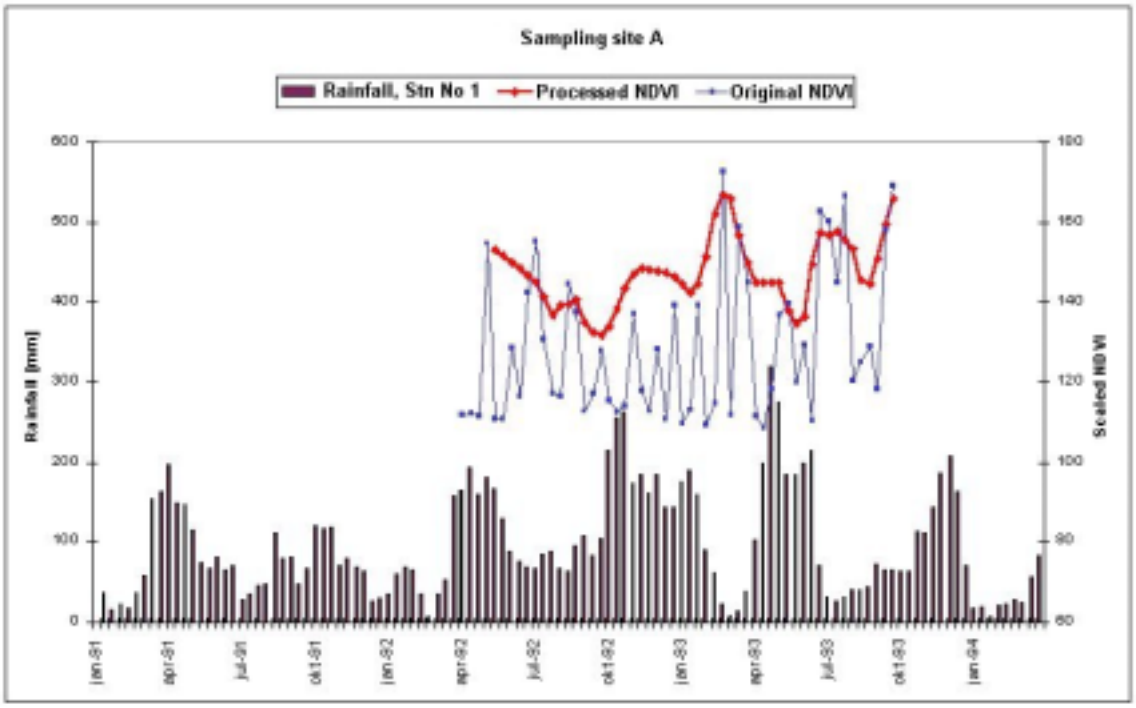

Figure 18. *Sampling site A is a bamboo forest on the west slope of Mt Kenya. Rainfall is aggregated over 10-day periods. Original NDVI data show the result before cloud detection, interpolation and the moving average of the 10-day composites. Processed NDVI show the result after applying these methods .*

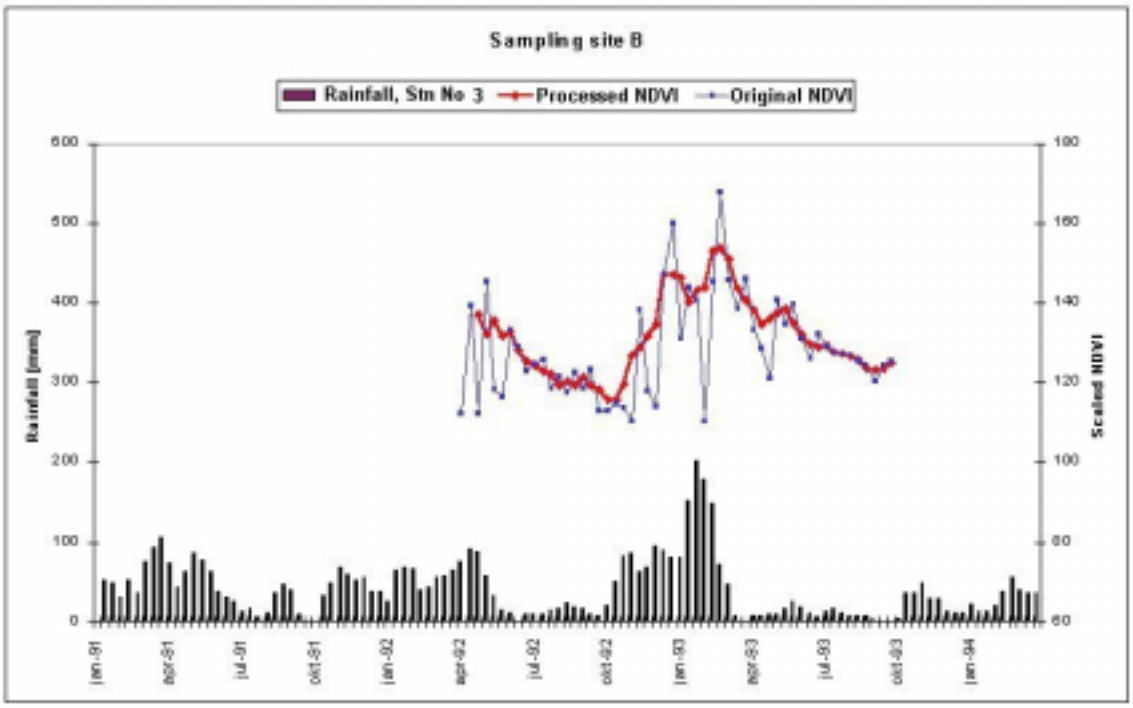

Figure 19. *Sampling site B is grassland on the west foot of Mt Kenya. Rainfall is aggregated over 10-day periods. Original NDVI data show the result before cloud detection, interpolation and the moving average of the 10-day composites. Processed NDVI show the result after applying these methods.*

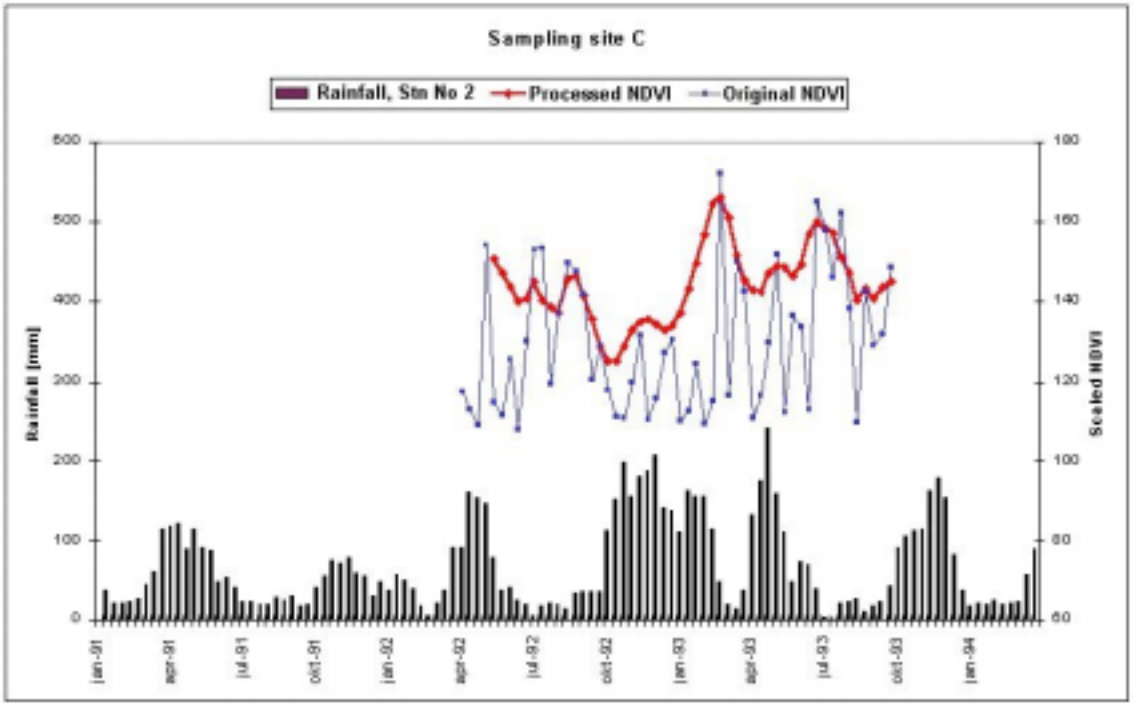

Figure 20. *Sampling site C is a montane evergreen forest on the west of Mt Kenya. Rainfall is aggregated over 10-day periods. Original NDVI data show the result before cloud detection, interpolation and the moving average of the 10-day composites. Processed NDVI show the result after applying these methods.*

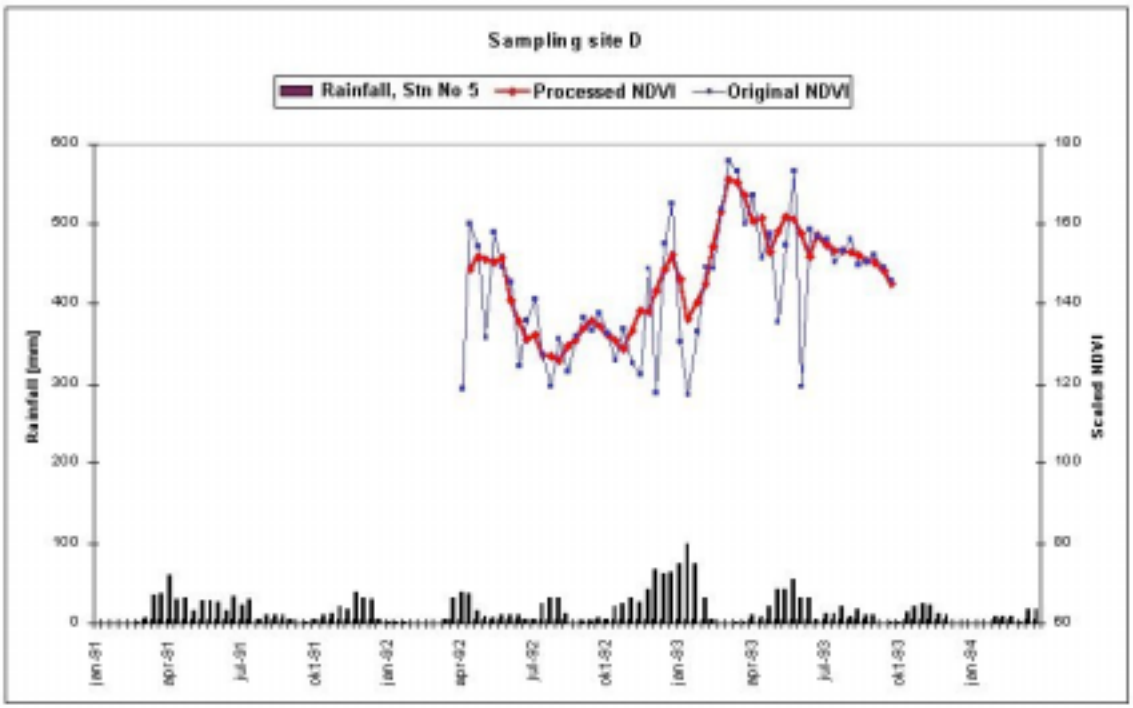

Figure 21. *Sampling site D is dry forest, Mokogodo forest, north of Mt Kenya. Rainfall is aggregated over 10-day periods. Original NDVI data show the result before cloud detection, interpolation and the moving average of the 10-day composites. Processed NDVI show the result after applying these methods.*

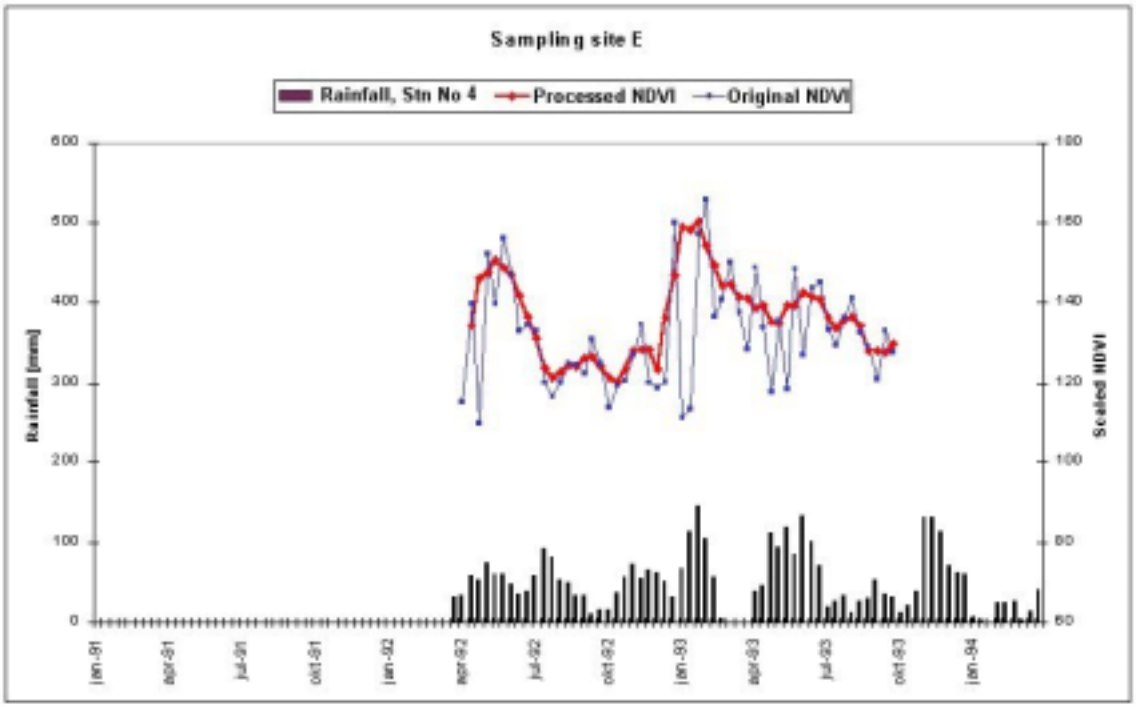

Figure 22. *Sampling site E is a cropland, on the north foot of Mt Kenya. Rainfall is aggregated over 10-day periods. Original NDVI data show the result before cloud detection, interpolation and the moving average of the 10-day composites. Processed NDVI show the result after applying these methods.*

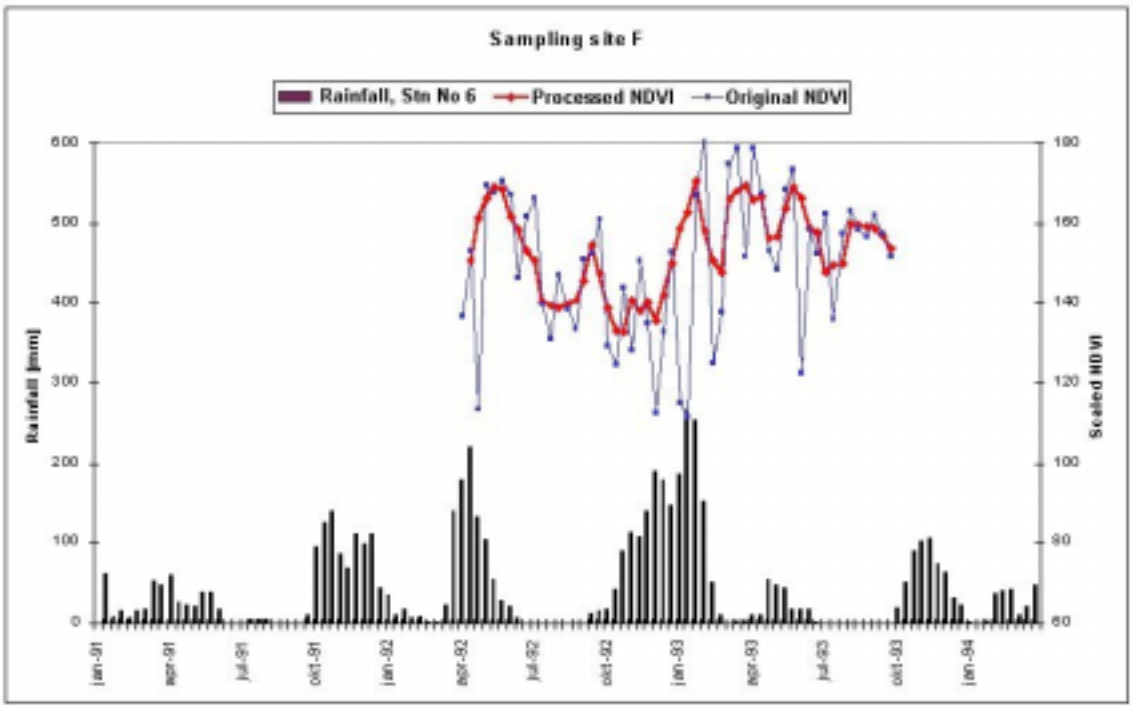

Figure 23. *Sampling site F is Meru forest, a moist semi deciduous forest on northeast of Mt Kenya. Rainfall is aggregated over 10-day periods. Original NDVI data show the result before cloud detection, interpolation and the moving average of the 10-day composites. Processed NDVI show the result after applying these methods.*

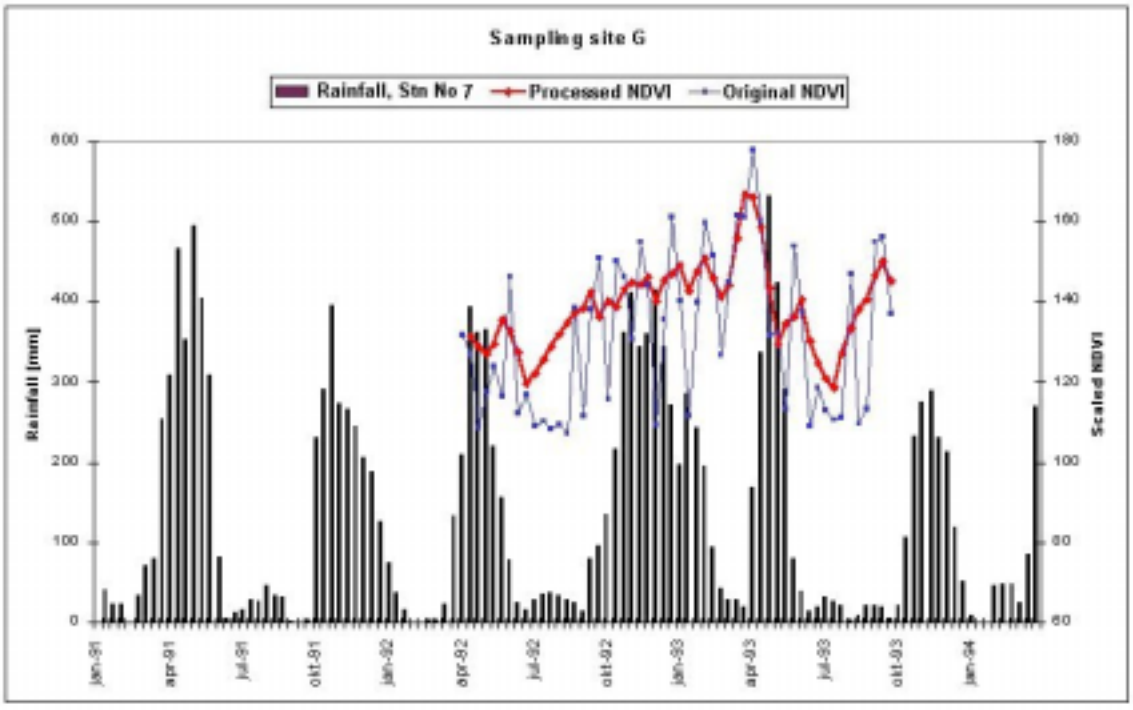

Figure 24. *Sampling site G is a montane evergreen forest on the east slope of Mt Kenya. Rainfall is aggregated over 10-day periods. Original NDVI data show the result before cloud detection, interpolation and the moving average of the 10-day composites. Processed NDVI show the result after applying these methods.*

For each sampling site, and for the whole time series, the number of cloud contaminated pixels were calculated (Table 7).

Table 7. *The percentage of cloud contaminated pixels from the total data set of 53 composites*

Sampling site	Missing values (%)
A (bamboo, west)	55
B (grassland, west	9
C (montane evergreen west)	45
D (dry forest, north)	2
E (cropland, north)	8
F (semideciduous, east)	9
G (montane evergreen east)	26

Table 8 summarises the information given in Figure 18-24

Table 8. *Describes the main peaks and drops in rainfall and NDVI, as well as the annual rainfall for each site.*

Study areas	**Annual rainfall (mm)**			**Peaks rainfall**	**Peaks NDVI**	**Drops rainfall**	**Drops NDVI**
	-91	-92	-93				
A Bamboo, west	2708	4227	4048	March-May -91, April-May -92, Oct 92-Jan 93, Apr-Jun -93, Nov-Dec- 93	Nov-Dec -92, Mar -93, Jun-Jul -93	May-Jul -91, Dec-91 Feb-92 Jun-Sept -92, Feb-Mar -93, Jul-Oct -93	Oct -92, May-Jun -93, Aug -93
B Grassland	1576	1629	1288	March, May -91, Nov -91, Jan -92, May -92, Oct 92-Feb -93	Dec -92, Mar -93	Sept-Oct -91, Jun-Sept -92, Mar-Oct -93,	Oct -92, April -93
C Montane Evergreen, west	1861	2812	3089	Apr-May -91, Oct -91, Apr-May -92, Oct-Feb -93, Apr-May -93, Oct-Dec -93	Aug –92, Jan-Feb –93, Jun –93	Jul-Sept -91, Feb -91, Jul-Aug 92, Feb –93, Jul-Sept -93	Sept-Oct –92, Apr –93, Aug –93
D Dry forest	613	639	740	Precipitation very low, minor peaks in Apr-91, Nov-91, Apr–92, Jul -92, Nov - Jan-93, May -93	May-92, Dec-92 - Jan-93, Mar -93	Little or no rainfall in Jan-91, Sept –91, Jan -Feb -92, Jun -92, Sept -92, Mar -93,Jul -93, Sept -93	Aug -92, Oct -92, Jan -93
E Cropland				Jan -93 Apr-Jun -93 Nov -93	May -92, Jan-Feb -93	Sept -92, Feb-Mar -93, Jul-Oct -93,	Jul-Dec -93, May -93, Oct -93
F Meru forest	1352	2048	1707	Oct -91, Apr -92, Nov -92- Jan -93,	May -92, Sept -92, Jan -93, Mar -93, Jun -93	Jun-Oct –91, Feb-Mar –92, Jun-Sept –92, Mar –93, Jul-Oct –93	Jul-, Oct -92, Mar-,May-, Jul-93
G Montane Evergreen, East	5367	5352	4737	Apr-Jun and Oct-Nov every year	Apr -93, Sept -93	Jun-Sept and Feb-Jan every year	Jun -92, May-, Jul -93

8 DISCUSSION

There were some important questions to take into consideration throughout this study. Did our results provide reliable representation of our selected sampling sites, regarding homogenous vegetation, area size and clouds? How representative were the precipitation stations to the correlated areas?

8.1 Temporal NDVI profiles

The results in Figures 18-24 show NDVI for each 10-day composite in each area before applying cloud detection methods and a moving average on interpolated three 10-composites after applying cloud detection. Fluctuations in the interpolated NDVI are shown for all the sampling sites, which are partially caused by clouds, as well as, due to vegetation seasonality (phenology). Also, common for all sampling sites was the short time series, which made it difficult to analyse any interannual variability.

A generalised NDVI temporal profile for vegetation rises as plant cover increases, reaches a peak or a plateau and falls off with plant senescence and death. Where the vegetation canopy changes very little with time, *e.g.*, tropical rainforests, the NDVI profile tends not to show marked rises and falls, but remains as a plateau. Thus NDVI profiles can provide a means of describing vegetation phenology. In addition, the dependence of NDVI on cover is known to vary between vegetation types. Therefore, different biomes are expected to have different NDVI profiles. NDVI profiles for a given vegetation type can vary from area to area and from year to year depending on the prevailing weather.

8.1.1 Sample sites A, C and G – evergreen vegetation

Sampling sites A (bamboo forest), C and G (montane evergreen forest) are biomes containing rich plant cover and are green all year. As mentioned above, the vegetation canopy changes very little with time. Thus in the case of sampling sites A, C and G, the NDVI profiles are expected to remain as a plateau. Consequently, the growing season is not easily detected. All the three sampling sites are highly influenced by clouds (Table 7). This can be seen by the strong fluctuation in the NDVI profiles.

On the east slope of Mount Kenya (site G), 26% of the original NDVI 10-day composites were flagged as cloudy and replaced by interpolated values. This is shown clearly in Figure 24 (a strong fluctuation in especially the original data), between June to August 92 and April to August 93.

In Figures 18 and 20 the monthly NDVI profiles have very high values compared to the original NDVI. This is because in sampling sites A (bamboo forest) and C (montane evergreen forest), 55% and 45% of the 10-composites have been interpolated respectively. The pixels flagged as cloudy, *i.e.* low NDVI are not included in the calculation of the monthly moving average graphs and therefore the monthly NDVI is calculated on very few “true“ pixels with a high NDVI. The frequent drops in NDVI for site A and C during the whole time series are due to clouds.

Figure 2 shows that two sampling sites of the same biome (vegetation composition) were chosen. Sampling site C on the west slope of Mount Kenya and sampling site G on the east slope both contained montane evergreen forest. This biome has a thick vegetation cover of three layers. The west sampling site (C) is located in the rain shadow of Mount Kenya, and therefore has a much lower annual rainfall than the sampling site (G) on the east slope. The eastern slope of Mt Kenya is very misty contributing to the humidity in addition to the large amount of annual rainfall. Montane evergreen forest on the east side has by far the highest amount of rainfall among our sampling sites. In spite of the large differences in rainfall and rainfall patterns, corresponding differences are not expected to be found in NDVI between sampling site C and G. This is because both areas are evergreen and are therefore not expected to show great differences in phenology.

Sampling site A (bamboo) is evergreen and very homogenous. This site is very small, about 2-3 km^2 and due to the high amount of clouds in the area, the resultant NDVI profile is not representative for bamboo.

It was not possible to make a separation between montane evergreen forest and bamboo. The biomes have continuously high rainfall in extremely cloudy areas. Sampling sites A and C are quite small and are situated very close, maybe too close to be able to separate them from one another. The NDVI profile for these biomes does not provide reliable representation for the selected features and therefore phenological information, such as the beginning and end of growing season, has not been defined.

8.1.2 Sample site F - Meru forest, semideciduous forest

Meru forest is semideciduous, which means that it contains both deciduous trees and bushes that will senescence and shred leaves and coniferous trees that stay evergreen. The forest is situated on the north-eastern slope of Mt Kenya and has high annual rainfall. The NDVI data for our time-series were therefore expected to be relatively high and even, and show a NDVI profile much as the sites discussed in section 8.1.1. The NDVI data in Figure 23 fluctuates, which we interpret as cloud interference. The amount of rainfall at Meru forest is expected to be as high as the montane evergreen forest on the east side. The result presented in Figure 23 shows much lower amounts. The rainfall data for Meru forest were received from Kisima farm (station no 6 in Figure 2). It is located on the border of the rain shadow on the west side. Therefore rainfall data from Kisima farm are probably not representative for Meru forest and the amounts of rainfall are probably higher than what is shown in Figure 23.

It was not possible to make a separation between Meru forest and montane evergreen forest or bamboo. Also, Meru forest is situated in an area with continuously high rainfall, and extremely high amounts of clouds. The NDVI profile for these biomes cannot be said to provide reliable representation for the selected feature.

8.1.3 Sample site B - grassland

For sampling site B (grassland), the temporal NDVI profile is expected to fluctuate with rainfall, in terms of a quick increase in NDVI after rainfall and low NDVI in dry periods due to thin vegetation. This area, west of Nanuyki, on the Laikipia plateau, has an annual rainfall between 750-1200 mm, with poor soil and low water capacity (Rooth 1995), which makes the area dry. The rainfall station for this area is actually west of the sampling site, but it is supposed to represent the area quite well. NDVI is responding to rainfall as expected, with a

peak in rainfall followed shortly by a peak in NDVI (Figure 19). The onset of the growing season begins around October-November in 1992 and starts to level off around April 1993. Reflection of vegetation is often mixed with that of soil surface (section 4.3.2). Dry, bright soil tends to have high reflectance both in the red and the infrared region, but low in the near infrared, in contrast to living vegetation, which is low in red and high in near infrared (Figure 15). The temporal NDVI is therefore negatively influenced (*i.e.* lower NDVI) which is shown during the dry season (June-October 92 and March-October 93) when the grass is senesced and the soil is dry.

8.1.4 Sample site D – dry forest

The area around Mokogodo forest represents the driest area of our sampling sites (D) with an annual rainfall of 500-600 mm. Rain is assumed to be the controlling factor for vegetation. The NDVI profile's onset and end of growing season are expected to fluctuate with rainfall. The response time in NDVI due to rainfall is expected to be longer for Mokogodo forest than for grassland. Trees have deeper root systems and thus do not absorb the water as quickly as grass. Mokogodo forest consists of two layers, one tree and one bush layer and therefore NDVI is expected to be higher than for grassland. The result corresponds well with our expectations. As shown in Figure 21 the start of the growing season is in November 92 with a sharp drop in January 93 most probably caused by clouds. The end of the growing season cannot clearly be seen, as the time series is too short. In May 1992, a drop in NDVI may indicate the end of the growing season, but clouds may also cause the drop. The rainfall station for Mokogodo station, number 5 in Figure 2, is well representative for the area in spite of being located east of the sampling site (personal communication with Laikipia Research Programme).

An interesting observation in the field was that Mokogodo forest (Figure 6) is a well-defined area and the vegetation differs greatly from the nearby surrounding area (Figure 7) that has the same amount of annual rainfall. In Mokogodo forest, the dominating species are *Juniperus* and *Olea* and these trees species are relatively drought resistant. The area surrounding Mokogodo forest has completely different vegetation, consisting of bush and heavily grazed areas. Species such as *Euphorbia*, which are very drought resistant, are found here. This might indicate that the forest has an additional water supply besides rainfall.

8.1.5 Sample site E - cropland

Wheat was being cultivated at the time of our field study. We do not show what crop was cultivated in 91-93, the time for our satellite data. For cropland, sampling site E, the NDVI is expected to show the local crop calendar *i.e.* the seasonal cycle of plowing, planting, emergence, growth, maturity, harvest and fallow. Each locality and each crop has its own crop calendar, defined by the interaction of the genetic character of the crop, the local climate and agricultural technology and tradition. As the area is artificially irrigated, NDVI is not expected to follow changes in rainfall. In Figure 22 the NDVI profile increases sharply in May 92 and in January 93, which can be interpreted as emergence and growth. NDVI decreases sharply in July 92 and more continuously from February 93. The first drop in NDVI may represent harvest, where the biomass is removed. The seasonal cycle may be discerned but influences from clouds are also present. This makes it difficult to distinguish the cycle from the clouds, especially on such a short time span. If there were no clouds, we would expect a more distinct pattern and sharper decreases.

8.2 Atmospheric influences

In applying the gross temperature test, the key point was in the definition of an appropriate threshold temperature. Over the sea it is relatively straightforward as the sea surface temperature varies slowly in space and time. Over land, however, the large temporal and spatial variability in surface temperatures, due to the different land uses and meteorological conditions, makes the definition of a single overall threshold temperature much more difficult.

The threshold was not easily set as channel 5 brightness temperature image covered a large area of Kenya which consists of major differences in temperature. At the top Mt Kilimanjaro and Mt Kenya the temperature is below zero in winter. We had no study areas at this altitude and therefore a value below zero would be too low to use as an appropriate threshold because then warm (above zero) clouds would not be eliminated. Satellite sensor data from our coldest sampling area were mostly influenced by clouds (especially during the winter) making it difficult to extract a threshold value.

A threshold of 280 Kelvin or 7 degrees Celsius was set by the following criteria. The brightness temperature image from July, the coldest month in Kenya, was displayed and we visually identified land areas that seemed likely to be the coldest, yet cloud-free surfaces in the image. The threshold value were then set a few Kelvin below the coldest area in the image, making sure that no land pixels were lower than the threshold value and thereby could be mistakenly classified as cloud pixel.

The result show that our data were still affected by clouds in spite of applying cloud detection methods. One of the reasons is that we only performed two out of APOLLO's five threshold sets. After applying these two tests on our data, around 50% of the information was lost (sampling site A and B), which meant that if we were to apply the remaining tests we would risk loosing more information. This resulted in having data which were still influenced by clouds. Unfortunately, we could not know the extent of cloud influence, which makes it difficult to determine the representativity for the area. Another reason of the limitation lies in the difficulty of reducing all noise and there are no methods that can give a 100% satisfactory result. Finally, the cloud detection method is limited in the case of very thin clouds and cloud fringes. Such configurations cannot be measured by temperature (Dreiser *et al*. 1991).

For the purpose of remote sensing one can generally say that all influences of the atmosphere increase with increasing scan angle of the sensor. At the AVHRR's maximum scan angle of 55.4° (off-nadir viewing), the path length through the atmosphere is 2.2 times longer than at nadir position (scan angle 0°) (Holben & Frazer 1984). To reduce atmospheric influences to a minimum it is recommended to use data only close to nadir.

The spectral bands in the AVHRR sensor are not ideal for vegetation monitoring, see Figure 15 on page 23. The main drawback is that channel 1 is too wide, and allows much more than photosynthetically active radiation into the sensor. Also, the gap between channel 1 and channel 2 is very small. It would be better if both channel 1 and 2 were narrower and if channel 2 were centred around the top of the reflectance curve in the NIR part.

The area around Mount Kenya is one of the cloudiest areas on the African continent, and has also been our major problem. We have been able to separate between major biomes like grassland and dry forest. We have not been able to extract representative NDVI profiles from

any of the selected biomes, mainly because of noise in the form of clouds. Phenological characteristics for sampling site B (grassland) and D (dry forest) were extracted. April 1:st 1992 to 21:st September 1993 is a very short time span to allow studies of vegetation seasonal characteristics and it is difficult to know whether the extracted NDVI profiles are representative for the surface in a longer time perspective.
For a more successfully result an area that is less influenced by clouds should be chosen.

9 CONCLUSIONS

The aim of this study was to investigate the usefulness of coarse resolution data from the NOAA AVHRR sensor for the identification and separation of biomes in Kenya, taking into consideration the influence of clouds on the quality of the remote sensing data.

Changes in AVHRR NDVI profiles should give an indication of changes in surface conditions, principally in the vegetation. However, there are nearly always undesirable noise in these profiles caused by cloud contamination, atmospheric variability and bi-directional effects.

Spectral radiance is strongly influenced by atmospheric conditions, *e.g.* clouds. Our study area, in the Kenyan highland, has an almost permanent cloud cover during the rain season, which often degrades the image quality. It is also important to identify the magnitude of uncertainty present in AVHRR data over time, such as scan angle, atmospheric effects and surface conditions.

Our study has shown that identification and separation of grassland and dry forest are possible. As expected grassland has low NDVI values during the dry season and responds with a quick increase in NDVI after rainfall compared to dry forest with deeper roots, which implies slower response to rainfall. We also found the highest NDVI values for moist semideciduous forest and decreasing NDVI for dry forest and grass. Phenological characteristics, such as beginning and end of the growing season, have only been possible to extract for grassland and dry forest. The NDVI profiles for all sampling sites can be doubted, due to large amount of clouds and the limited time series. For further phenological studies, areas less affected by clouds and longer time series of satellite data, as they become available, should be used.

Acknowledgements

This Master of Science thesis was completed at the Department of Physical Geography at Lund University. The field study was carried out in June – July 1998.

We want to give our special thanks to our supervisor Dr. Lars Eklundh at the Department of Physical Geography at Lund University for invaluable advice and encouragement throughout the project.

The field study was carried out during two months in Kenya. We are very grateful to our supervisor in Kenya, Dr. Francis Gichuki at the Department of Agricultural Engineering at University of Nairobi and his team at the Laikipia Research Programme, who welcomed us and provided us with ideas and precipitation data.

Without the help from The Swedish International Development Agency (Sida) this study would not have been realized. A special thanks to the Centre of International Environment Studies, (CIES), at the Royal Institute of Technology, KTH, who granted us a MFS scholarship.

Thank you Fredrik for being an excellent driver and photographer and thank you Martin for the support and encouragement needed to complete this study.

We wish to thank Kristin Andersson, Carin Kjellander, Tarek Rashed, and Birgitta and Håkan Schmidt for having contributed with advices and helped with scientific and /or linguistic issues.

Finally, we wish to thank all the people that have helped us throughout the study and made our stay in Kenya an experience of a lifetime.

References

Achard, F., and Blasco, F., 1990, Analysis of Vegetation Seasonal Evolution and Mapping of Forest Cover in West Africa with the Use of NOAA AVHRR HRPT Data, *Photogrammetric Enineering and Remote Sensing*, 56, pp 1359-1365.

Berger, F. H., 1995, The variability of clound cover and clound forcing inferred from NOAA AVHRR data for the north sea, *Advances in Space Research*, vol. 16, 10:29-32.

Campbell, J. B., 1996, *Introduction to remote sensing*, 3rd edition. Taylor & Francis Ltd, London, 622 pp.

Cihlar, J., Li, Z., Zheng, X., Moreau, L., Ly, H., 1996, The bidirectional Effects of AVHRR Measurements over Boreal Regions, *IEEE Transactions on geoscience and remote sensing*, vol. 34:6

Dreiser, C., Eiden, G., Gesell, G., König, T., 1991, *Range Management Handbook of Kenya*, vol. III/4, Ministry of Livestock Development, Range Management Division, Nairobi.

Eastman, J. R., 1993, *IDRISI version 4.1, Update manual*, Clark University, Worcester.

Eidenshink, J. C., and Faundeen, J. L., 1994, The 1-km AVHRR global land dataset: first stages in implementation, *International Journal of Remote Sensing*, vol. 15, pp 3443-3462.

Eidenshink, J. C., and Faundeen, J. L., 1995, The 1-km AVHRR global land dataset: first stages in implementation.
[Available on-line from http://edcwww.cr.usgs.gov/landdaac/1KM/paper/html]

Eklundh, L., 1996, *AVHRR NDVI for monitoring and mapping of vegetation and drought in East African environments*, Meddelanden från Lunds Universitets Geografiska Institution, Avhandlingar 126, Ph.D. thesis, University of Lund, Lund, 182 pp.

Herlocker, D. J., and Thurow, T. L., 1993, *Range Management Handbook of Kenya, volume III/5*, Ministry of Agriculture, Livestock Development and Marketing, Nairobi.

Holben, B. N. and Frazer, R. S., 1984. Red and near-infrared sensor response to off-nadir viewing, *International Journal of Remote Sensing*, vol. 5,
pp 145-160.

Holben, B. N, 1986, Characteristics of maximum-value composite images from temporal AVHRR data, *International Journal of Remote Sensing*, vol. 7,
pp 1417-1434.

Hutchison, K. D. and Hardy, K. R., 1995, Threshold functions for automated cloud analyses of global meteorological satellite imagery, *International Journal of Remote Sensing*, vol. 16, pp 3665-3680.

International Soil Conservation Organization (ISCO), 6th *International soil conservation conference on Soil conservation for survival, 6th – 18th November 1989*, pre-conference tour in

Kenya 6th – 9th November 1989, excursion guide, Permanent Presidential Commission on Soil Conservation and Afforestation, Nairobi

Justice, C. O., Townshend, J.R.G., Holben, B. N., Tucker, C. J., 1985, Analysis of the phenology of global vegetation using meteorological satellite data, *International Journal of Remote Sensing*, vol. 6, pp 1271-1318.

Kriebel, K. T., 1996, Cloud detection using AVHRR data, *Advances in the Use of NOAA AVHRR Data for Land Applications*, pp 195-210.

Lillesand, T., and Kiefer, R. W., 1987, *Remote sensing and image interpretation*, 2nd edition, John Wiley & Sons, Inc., Singapore, 721 pp.

Lillesand, T., and Kiefer, R. W., 1994, *Remote sensing and image interpretation*, 3nd edition, John Wiley & Sons, Inc., New York.

Lind, E. M., and Morrisson, E. S., 1974, *East African Vegetation*, Longman Group Ltd, London, 237 pp.

Lundgren, B., 1975, *Land use in Kenya and Tanzania*, Royal College of Forestry, Stockholm, 354 pp.

Lundgren, L., 1992, *Miljöprofil Kenya*, report No 3, published by SIDA's Regional Soil Conservation Unit, RSCU, Nairobi.

Malingreau, J. P., 1986, Global vegetation dynamics: satellite observations over Asia, *International Journal of Remote Sensing*, vol. 7, pp 1121-1146

Malingreau, J. P. and Tucker, C. J., 1988, Large-scale deforestation in the southern Amazon basin of Brazil, *Ambio*, vol. 17, pp 49-55.

Malingreau, J. P., Tucker, C. J., Laporte, N., 1989, AVHRR for monitoring global tropical deforestation, *International Journal of Remote Sensing*, vol. 10, pp 855-867.

NASA; AVHRR NDVI composites available on-line at *http://edcdaac.usgs.gov/1KM/*,

Nämden för skoglig fjärranalys, 1993, *Flygbildsteknik och Fjärranalys*, Skogsvårdsstyrelsen.

Ojany, F. F., and Ogendo, R. B., 1988, *Kenya: A Study in Physical and Human Geography*, Longman Kenya Ltd, Nairobi, 225 pp.

Olsson, L and Eklundh, L., 1994, *Fourier Series for analysing of temporal sequenses of satellite sensor imagery*, International Journal of Remote Sensing, vol. 15, pp 3735-3741.

PCI, 1994, *Using PCI Software, Version 5.3 EASI/PASE*, PCI., Inc, Richmond Hill.

Prince, S.D ., and Tucker, C. J., 1986, Monitoring the grasslands of the Sahel 1984-1985, *International Journal of Remote Sensing*, vol. 7, pp 1571-1581.

Reader, J., 1989, *Mount Kenya*, Elm Tree Books, Great Britain.

Reed, B. C., Brown J.F., VanderZee, D., Loveland, T.R., Merchant, J.W., Ohlen, D.O., 1994, Measuring phenological variability from satellite imagery, *Journal of vegetation science*, 5:703-715, Opulus Press Uppsala, Sweden.

Reed, B. C and Schwartz, M. D., 1999, Surface phenology and satellite sensor-derived onset of greenness: an initial comparison, *International Journal of Remote Sensing*, vol. 20, pp 3451-3457.

Ringrose, S., Matheson, W., Mgotsi, B. and Tempset, F., 1989, The Darkening Effect in Drought Affected Savanna Woodland Environment Relative to Soil Reflectance in Landsat and SPOT Wavebands, *Remote Sensing of Environment*, vol. 30, 1:1-19

Roth, S., 1997, *Land Use Classification of the Upper Ewaso Ngíro Basin in Kenya by means of Landsat TM Satellite Data*, Master Thesis, University of Berne, Berne, 126 pp.

Saunders, R.W., and Kriebel, K. T., 1988, An Improved Method for Detecting Clear Sky and Cloudy Radiances from AVHRR Data, *International Journal of Remote Sensing*, vol. 9, pp 123-150.

Schwartz, M.D., 1999, Advancing to full bloom; planning phenological research for the 21st century, *International Journal of Biometeorology*, vol. 42, pp 113-118.

Schwartz, M.D. and Reed, B.C., 1999, Surface phenology and satellite sensor-derived onset of greenness: an initial comparison, *International Journal of Remote Sensing*, vol. 20, pp 3451-3457.

Stowe, L.L., E.P. McClain, R. Carey, P. Pellegrino, G. G. Gutman, P. Davis, C. Long, and S. Hart, 1991, Global distribution of cloud cover derived from NOAA/AVHRR operational satellite data, *Advances in Space Research*, vol. 11, 3:51-54.

Swain, P. H. and Davis, S. M. (eds), 1978, *Remote Sensing – The Quantitative Approach*, McGraw-Hill, New York.

Townshend, J. R. G., Justice, C., Li, W., Gurney, C. and McManus, J., 1991, Global land cover classification by remote sensing: present capabilities ant future possibilities, *International Journal of Remote Sensing*, vol.35, pp 243-255.

Townshend, J. R. G. and Justice, C. O., 1990, The spatial variation of vegetation changes at very coarse scales, *International Journal of Remote Sensing*, vol. 11, pp 149-157.

Tucker, C. J., 1979, Red and photographic infrared linear combinations for monitoring vegetation, *Remote sensing of Environment*, 8:127-150

Tucker, C. J., Gatlin, J. A., and Schneider, S. R., 1984, Monitoring Vegetation in the Nile Delta with NOAA-6 and NOAA-7 AVHRR Imagery, *Photgrammetric Engineering and Remote Sensing*, vol. 50, pp 53-61

Tucker, C. J. and Sellers, T. J., 1986, Satellite remote sensing of primary production, *International Journal of Remote Sensing*, vol. 7, pp 1395-1416.

Zhu, Z. -L and Yang, L., 1996, Characteristics of the 1 km AVHRR data set for North America, *International Journal of Remote Sensing*, vol. 17, pp 1915-1924.

Personal communication; Joseph K Mitugo, Laikipia Research Programme, Kenya.

This flowchart summarises the methods used to get result from original NDVI as well as from processed data, after cloud detection and interpolation. The set numbers are just an example and the shaded 'hand draw' area symbolises a sampling site.

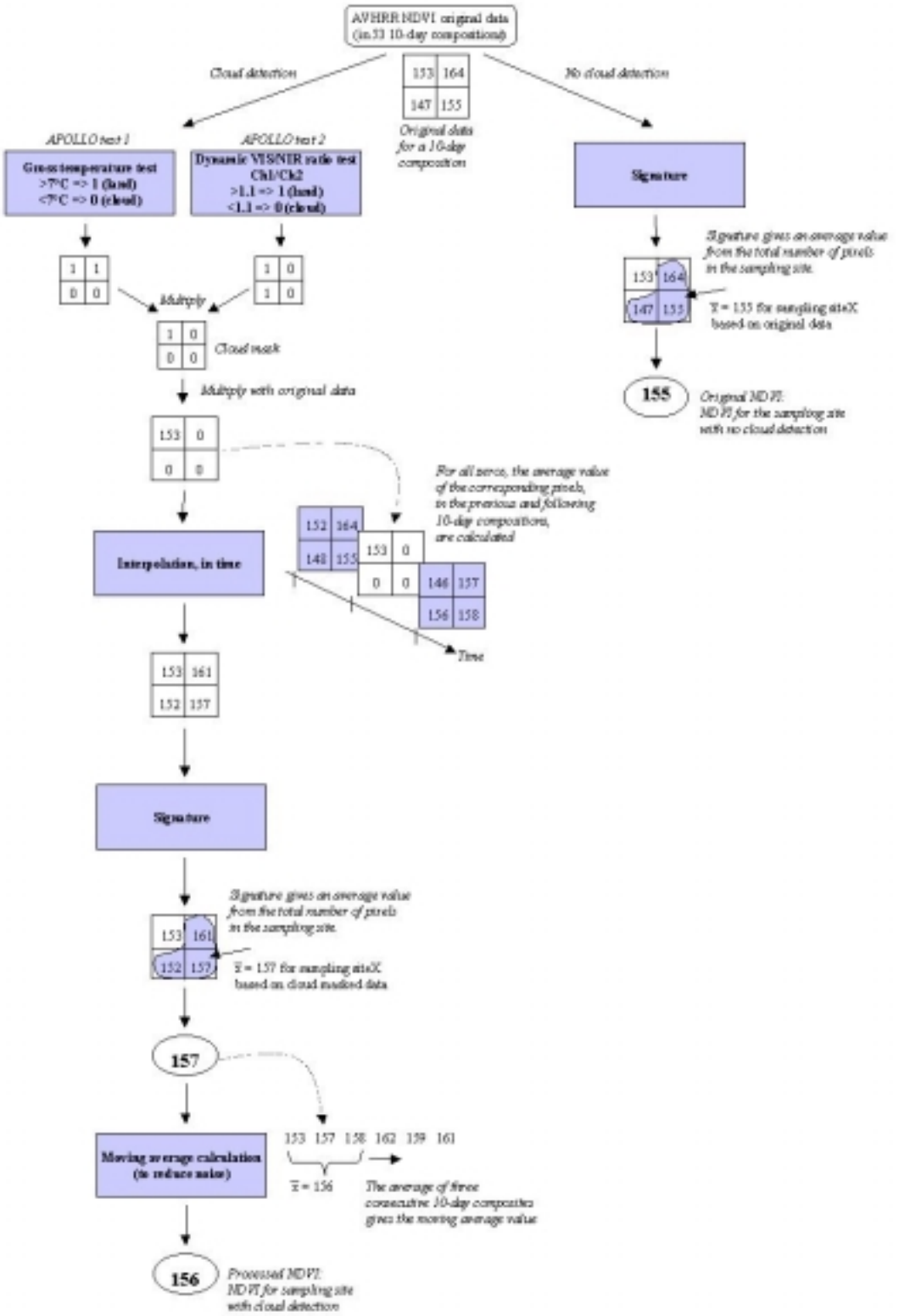

Abbreviations and terminology

APOLLO	AVHRR Processing scheme Over Clouds, Land and Ocean
AVHRR	Advanced Very High Resolution Radiometer
BRDF	Reflection characteristics of a surface are described by the Bidirectional Reflectance Distribution Function
Biome	A climatically controlled group of plants and animals of a characteristic composition and distributed over a wide area, such as tropical rainforest, temperate grassland, desert, savannah and mountain habitats etc.
CLAVR	Clouds from AVHRR
GPS	Global Positions System
IFOV	Instantaneous Field of View
MIR	Middle infrared
MSS	Multispectral Scanner
MVC	Maximum Value Composite
Nadir	Ground nadir is the point on the surface that are exactly underneath the centre of the lens in the sensor.
NDVI	Normalised Difference Vegetation Index
NIR	Near infrared
NOAA	National Oceanic and Atmospheric Administration
Phenology	Seasonal pattern for vegetation. The phenology of a specific plant defines its seasonal pattern of growth, flowering, senescence and dormancy.
Pixel	A satellite scene consist of pixels, where one pixel is the ground resolution.
Taxa	Individual classification groups for both plants and animals

Temporal NDVI profile	NDVI values graphed over time. Different vegetation types can be distinguished by the differences in spectral reflectance over time.
Vegetation signature	Spectral reflectance for vegetation.
VIS	Visible

Lunds Universitets Naturgeografiska institution. Seminarieuppsatser. Uppsatserna finns tillgängliga på Naturgeografiska institutionens bibliotek, Sölvegatan 13, 223 62 LUND.

The reports are available at the Geo-Library, Department of Physical Geography, University of Lund, Sölvegatan 13, S-223 62 Lund, Sweden.

1. Pilesjö, P. (1985): Metoder för morfometrisk analys av kustområden.
2. Ahlström, K. & Bergman, A. (1986): Kartering av erosionskänsliga områden i Ringsjöbygden.
3. Huseid, A. (1986): Stormfällning och dess orsakssamband, Söderåsen, Skåne.
4. Sandstedt, P. & Wällstedt, B. (1986): Krankesjön under ytan - en naturgeografisk beskrivning.
5. Johansson, K. (1986): En lokalklimatisk temperaturstudie på Kungsmarken, öster om Lund.
6. Estgren, C. (1987): Isälvsstråket Djurfälla-Flädermo, norr om Motala.
7. Lindgren, E. & Runnström, M. (1987): En objektiv metod för att bestämma läplanteringars läverkan.
8. Hansson, R. (1987): Studie av frekvensstyrd filtringsmetod för att segmentera satellitbilder, med försök på Landsat TM-data över ett skogsområde i S. Norrland.
9. Matthiesen, N. & Snäll, M. (1988): Temperatur och himmelsexponering i gator: Resultat av mätningar i Malmö.

10A. Nilsson, S. (1988): Veberöd. En beskrivning av samhällets och bygdens utbyggnad och utveckling från början av 1800-talet till vår tid.

10B. Nilson, G., 1988: Isförhållande i södra Öresund.

11. Tunving, E. (1989): Översvämning i Murciaprovinsen, sydöstra Spanien, november 1987.
12. Glave, S. (1989): Termiska studier i Malmö med värmebilder och konventionell mätutrustning.
13. Mjölbo, Y. (1989): Landskapsförändringen - hur skall den övervakas?
14. Finnander, M-L. (1989): Vädrets betydelse för snöavsmältningen i Tarfaladalen.
15. Ardö, J. (1989): Samband mellan Landsat TM-data och skogliga beståndsdata på avdelningsnivå.
16. Mikaelsson, E. (1989): Byskeälvens dalgång inom Västerbottens län. Geomorfologisk karta, beskrivning och naturvärdesbedömning.
17. Nhilen, C. (1990): Bilavgaser i gatumiljö och deras beroende av vädret. Litteraturstudier och mätning med DOAS vid motortrafikled i Umeå.
18. Brasjö, C. (1990): Geometrisk korrektion av NOAA AVHRR-data.
19. Erlandsson, R. (1991): Vägbanetemperaturer i Lund.
20. Arheimer, B. (1991): Näringsläckage från åkermark inom Brååns dräneringsområde. Lokalisering och åtgärdsförslag.
21. Andersson, G. (1991): En studie av transversalmoräner i västra Småland.

22A. Skillius, Å., (1991): Water havesting in Bakul, Senegal.

22B. Persson, P. (1991): Satellitdata för övervakning av höstsådda rapsfält i Skåne.

23. Michelson, D. (1991): Land Use Mapping of theThat Luang - Salakham Wetland, Lao PDR, Using Landsat TM-Data.

24. Malmberg, U. (1991): En jämförelse mellan SPOT- och Landsatdata för vegetationsklassning i Småland.
25. Mossberg, M. & Pettersson, G. (1991): A Study of Infiltration Capacity in a Semiarid Environment, Mberengwa District, Zimbabwe.
26. Theander, T. (1992): Avfallsupplag i Malmöhus län. Dränering och miljöpåverkan.

27. Osaengius, S. (1992): Stranderosion vid Löderups strandbad.
28. Olsson, K. (1992): Sea Ice Dynamics in Time and Space. Based on upward looking sonar, satellite images and a time series of digital ice charts.
29. Larsson, K. (1993): Gully Erosion from Road Drainage in the Kenyan Highlands. A Study of Aerial Photo Interpreted Factors.
30. Richardson, C. (1993): Nischbildningsprocesser - en fältstudie vid Passglaciären, Kebnekaise.
31. Martinsson, L. (1994): Detection of Forest Change in Sumava Mountains, Czech Republic Using Remotely Sensed Data.
32. Klintenberg, P. (1995): The Vegetation Distribution in the Kärkevagge Valley.
33. Hese, S. (1995): Forest Damage Assessment in the Black Triangle area using Landsat TM, MSS and Forest Inventory data.
34. Josefsson, T. och Mårtensson, I. (1995). A vegetation map and a Digital Elevation Model over the Kapp Linné area, Svalbard -with analyses of the vertical and horizontal distribution of the vegetation
35. Brogaard, S och Falkenström, H. (1995). Assessing salinization, sand encroachment and expanding urban areas in the Nile Valley using Landsat MSS data.
36. Krantz, M. (1996): GIS som hjälpmedel vid växtskyddsrådgivning.
37. Lindegård, P. (1996). VINTERKLIMAT OCH VÅRBAKSLAG. Lufttemperatur och kådflödessjuka hos gran i södra Sverige.
38. Bremborg, P. (1996). Desertification mapping of Horqin Sandy Land, Inner Mongolia, by means of remote sensing.
39. Hellberg, J. (1996). Förändringsstudie av jordbrukslandskapet på Söderslätt 1938-1985.
40. Achberger, C. (1996): Quality and representability of mobile measurements for local climatological research.
41. Olsson, M. (1996): Extrema lufttryck i Europa och Skandinavien 1881-1995
42. Sundberg, D. (1997): En GIS-tillämpad studie av vattenerosion i sydsvensk jordbruksmark.
43. Liljeberg, M. (1997): Klassning och statistisk separabilitetsanalys av marktäckningsklasser i Halland, analys av multivariata data Landsat TM och ERS-1 SAR.
44. Roos, E. (1997): Temperature Variations and Landscape Heterogeneity in two Swedish Agricultural Areas. An application of mobile measurements.
45. Arvidsson, P. (1997): Regional fördelning av skogsskador i förhållande till mängd SO_2 under vegetationsperioden i norra Tjeckien.
46. Akselsson, C. (1997): Kritisk belastning av aciditet för skogsmark i norra Tjeckien.
47. Carlsson, G. (1997): Turbulens och supraglacial meandring.
48. Jönsson, C. (1998): Multitemporala vegetationsstudier i nordöstra Kenya med AVHRR NDVI
49. Kolmert, S. (1998): Evaluation of a conceptual semi-distributed hydrological model – A case study of Hörbyån.
50. Persson, A. (1998): Kartering av markanvändning med meteorologisk satellitdata för förbättring av en atmosfärisk spridningsmodell.
51. Andersson, U. och Nilsson, D. (1998): Distributed hydrological modelling in a GIS perspective – an evaluation of the MIKE SHE model.
52. Andersson, K. och Carlstedt, J. (1998): Different GIS and remote sensing techniques for detection of changes in vegetation cover - A study in the Nam Ngum and Nam Lik catchment areas in the Lao PDR.
53. Andersson, J., (1999): Användning av global satllitdata för uppskattning av spannmålsproduktion i västafrikanska Sahel.
54. Flodmark, A.E., (1999): Urban Geographic Information Systems, The City of Berkeley

Pilot GIS

55A. Lyborg, Jessic & Thurfell, Lilian (1999): Forest damage, water flow and digital elevation models: a case study of the Krkonose National Park, Czech Republic.

55B. Tagesson, I., och Wramneby, A., (1999): Kväveläckage inom Tolångaåns dräneringsområde – modellering och åtgärdssimulering.

56. Almkvist, E., (1999): Högfrekventa tryckvariationer under de senaste århundradena.

57. Alstorp, P., och Johansson, T., (1999): Översiktlig buller- och luftföroreningsinventering i Burlövs Kommun år 1994 med hjälp av geografiska i informationssystem – möjligheter och begränsningar.

58. Mattsson, F., (1999): Analys av molnklotter med IRST-data inom det termala infraröda våglängdsområdet

59. Hallgren, L., och Johansson, A., (1999): Analysing land cover changes in the Caprivi Strip, Namibia, using Landsat TM and Spot XS imagery.

60. Granhäll, T., (1999): Aerosolers dygnsvariationer och långväga transporter.

61. Kjellander, C., (1999): Variations in the energy budget above growing wheat and barley, Ilstorp 1998 - a gradient-profile approach

62. Moskvitina, M., (1999): GIS as a Tool for Environmental Impact Assessment - A case study of EIA implementation for the road building project in Strömstad, Sweden

63. Eriksson, H., (1999): Undersökning av sambandet mellan strålningstemperatur och NDVI i Sahel.

64. Elmqvist, B., Lundström, J., (2000): The utility of NOAA AVHRR data for vegetation studies in semi-arid regions.

65. Wickberg, J., (2000): GIS och statistik vid dräneringsområdesvis kväveläckagebeskrivning i Halland

66. Johansson, M., (2000): Climate conditions required for re-glaciation of cirques in Rassepautasjtjåkka massif, northern Sweden.

67. Asserup, P., Eklöf, M., (2000): Estimation of the soil moisture distribution in the Tamne River Basin, Upper East Region, Ghana.

68. Thern, J., (2000): Markvattenhalt och temperatur i sandig jordbruksmark vid Ilstorp, centrala Skåne: en mätnings- och modelleringsstudie.

69. Andersson, C., Lagerström, M., (2000): Nitrogen leakage from different land use types - a comparison between the watersheds of Graisupis and Vardas, Lithuania.

70. Svensson, M., (2000): Miljökonsekvensbeskrivning med stöd av Geografiska Informationssystem (GIS) – Bullerstudie kring Malmö-Sturup Flyplats.

71. Hyltén, H.A., Uggla, E., (2000): Rule.Based Land Cover Classification and Erosion Risk Assessment of the Krkonoše National Park, Czech Republic.

72. Cronquist, L., Elg, S., (2000): The usefulness of coarse resolution satellite sensor data for identification of biomes in Kenya.